Towards Accurate Simulations of Space-Based Solar Power

Jack Mcnish

Department of Civil and Environmental Engineering
Imperial College London

Abstract

Space-based solar power (SBSP), collecting energy in space and beaming it to Earth, has the potential to revolutionize the energy industry with it's unique ability to provide a continuous source of renewable energy. Accurately calculating the energy generation of such systems is complex and relies on non-trivial simulations, but cost-benefit studies ignore these intricacies leading to potentially erroneous values and false conclusions. Calculating the solar power satellites receive in orbit has previously been studied in the literature, but these approaches are not directly relevant to SBSP systems, not taking into account line-of-sight between the satellite and the ground station, and not computing the resultant energy. This study establishes novel techniques for calculating the energy from SBSP systems, outlining two methodologies for calculating the energy potential of such systems depending on the available parameters; the first method allows energy simulations of SBSP systems as described by their wattage, with the second method studying SBSP from a more fundamental approach. Finally, sensitivity analyses of components like orbit and solar cell choice are conducted. This paper also resulted in the publication of an open-source Python package "sspPy" allowing anyone to compute power and energy curves of space-based solar power.

1. Introduction

Since the 7th century B.C., humans have harnessed the power of the Sun, beginning with the use of a magnifying glass to concentrate the sun's rays to make fire (N.R.E.L, n.d.); progress has continued, and in 1883, Charles Fritts created the first device to generate electricity from sunlight with selenium cells, which he documents in his paper "On a New Form of Selenium Cell" (1883). Space-based solar power (SBSP) is a newer concept, which aims to collect solar energy in space and beam it down to Earth. This typically consists of two main components: a solar power satellite (SPS), equipped with a solar array to collect the Sun's energy, and a ground antenna to receive the energy from the satellite.

The concept first appeared in the science-fiction story "Reason" by Isaac Asimov (1941) which depicts a solar station transmitting energy to different planets via microwave beams. It was later established in the scientific literature when Peter Glaser published "Power from the Sun: Its Future" in 1968, which demonstrated how energy could be transmitted from a solar satellite to Earth. Directly after this, research into space-based solar power erupted, with the concept being thoroughly investigated by NASA during a $50 million study "Satellite Power System Concept Development and Evaluation Program" between 1977 and 1981 but concluding that the technology was not yet developed enough to be viable (N.A.S.A, 1978). Over a decade later, NASA conducted a re-examination of space-based solar power with its "Fresh Look" study between 1995 and 1997 (Mankins, 1997) which found that space-based solar power was closer to reality than previously thought, but more work would be needed to develop the infrastructure to make it a reality. Within the past 5 years, there has been a revival in the concept, the United States (US) and China have built experimental prototypes, developed roadmaps, and commissioned feasibility studies; with other countries such as the United Kingdom still in the concept development stage.

Whilst research into space-based solar power has evolved over the last 50 years, work has focused primarily on two axes: since its invention in 1968, papers are focused on developing various SBSP concepts, the most recent state of the art concepts are SPS-Alpha by John Mankins (2012) and CASSIOPeiA by Ian Cash (Cash, 2019). There has also been a recent trend in cost-benefit analyses, with studies commissioned by the European Space Agency (E.S.A) from Frazer-Nash and Roland Berger (E.S.A, n.d.).

One of the principal challenges associated with such cost-benefit studies is accurately predicting the energy that can be generated from space-based solar power concepts, often these calculations are not detailed in the reports leading to doubt over their validity. Energy calculations for such concepts are complex, depending on a multitude of factors relating to the satellite's solar array and hardware, and the relative position of the Sun, the Earth receiving antenna and the satellite. These complexities make the development of analytical approaches to this task difficult, driving the need for simulation and computational-based approaches. This need is further emphasized by the amount of information simulations and modelling can offer. In deriving these models, data on a satellites position, its temperature, its power, and energy generation values are computed; data which can be useful for mission planning purposes, for example, to optimise solar array maintenance whilst the satellite is in the Earth's shadow.

There is previous literature detailing similar approaches as conducted in this paper, such as Etchell's "Developing a Power Modelling Tool for CubeSats" (2019) or "Calculating electric power generated by 3U CubeSat's photoconverters depending the orbit and orientation parameters" (Gorev *et al.*, 2019). However, these are not directly relevant to space-based solar power implementations as they fundamentally represent an entirely different architecture. There is no published research detailing energy calculation methodologies for space-based solar power concepts. This paper aims to address this gap by developing methodologies to calculate the energy generation potential of various space-based solar power implementations. The modelling methods have been designed to incorporate theory with real-world data wherever possible for accurate results.

This study firstly reviews the literature surrounding space-based solar power as well as methods of modelling such systems; following this, the methodology and chosen approaches made whilst simulating and calculating the energy potential of SBSP concepts are detailed, as well as the reasoning behind certain choices. Thirdly, the results are presented and discussed before scoping future work which could be done based on this study, finally, concluding remarks are made.

2. Literature Review

2.1. Origins of space-based solar power

Initial Concept

The idea of space-based solar power (SBSP) first appeared in 1941 in a science fiction story entitled "Reason" by Isaac Asimov, which describes a "solar station" in space, capable of gathering sunlight and beaming the energy to different planets (Asimov, 1941). The concept was later established scientifically when Peter Glaser published "Power from the Sun: Its Future" in 1968; the paper presents the concept of satellites in orbit around Earth equipped with solar collectors, receiving the Sun's energy and beaming it down to Earth. The concept called for two solar collecting satellites equipped with transmitting dish antennas, located in geostationary orbit, that would beam the collected energy in the form of microwave radiation, which would be collected by an Earth receiving station antenna (Glaser, 1968).

Benefits

The concept of collecting solar energy in space and beaming it to Earth has multiple benefits over other energy sources, notably traditional Earth-based solar, which makes the concept attractive as a future renewable energy source. Collecting solar energy in space, outside of Earth's atmosphere, rather than on the ground, results in energy collection which is unhindered by factors such as cloud cover, weather patterns, dust deposits and attenuation of solar energy by the atmosphere (Glaser, 1968). This results in solar panels receiving greater solar intensity in space than on Earth. Additionally, the proportion of time the solar power satellites spend illuminated by the Sun can be selected, unlike on Earth, with geosynchronous orbits being able to provide near-continuous solar illumination, as reported by Glaser in 1968 stating that the satellites would pass through the Earth's shadow once per day at an orbit of 35, 700 kilometers; this proportion is estimated to be over 99% as reported by Frazer-Nash in it's "Space Based Solar Power" report (Frazer-Nash, 2021). The ability to receive and thus beam energy to Earth quasi-continuously means space-based solar power can be a baseload energy source, in fact, this would make it the only renewable energy source to fulfil this criteria.

2.2. Principal components of space-based solar power

There are several categorizations of the main components of space-based solar projects, Vedda (2020) proposes splitting the components into a solar power satellite and a receiving system which can be terrestrial or in-space; however this breakdown does not account for the infrastructure necessary for orbital launch and assembly, these systems are taken into account by Frazer-Nash with their system architecture including a solar power satellite and a ground station, alongside operation and support engineering systems as well as complete lifecycle engineering systems and other controls and enablers (Frazer-Nash, 2021). Finally, John Mankins, inventor of the SPS-Alpha design, conceptualizes space-based solar power components into the following categories: Primary solar power satellite (SPS) platform systems, Secondary SPS platform systems, Ground systems and Supporting systems (Mankins, 2012). These three approaches have their own benefits, but in this literature review, the granular approach of Mankins has been selected as it does not group all in-space functions such as collecting power, wireless power transmission and propulsion systems into the singular entity of a solar power satellite; this detachment of functions appears in certain designs such as Mclinko's distributed cluster concept (2010).

2.3. Implementation scenarios of space-based solar power

Orbit Selection

Since Peter Glaser's initial paper, much research has gone into studying the benefits and limitations of various orbit choices, despite this, almost all SBSP research concludes that geosynchronous orbits are optimal, or use such orbits to model SBSP; this is because the satellites would be in near-continuous sunlight, as highlighted above; an added benefit is that the satellites would stay over the same spot in the sky, allowing their transmitting antennas to keep a virtually unchanged orientation, as stated by Ian Cash (2019) and Ryan McLinko (2010). Specific SBSP designs using geostationary / geosynchronnous orbits include the two current state-of-the-art concepts: SPS-Alpha by John Mankins (2012) and CASSIOPeia by Ian Cash (2019), as well as the Multi-Rotary Joints SPS design (Hou *et al.*, 2021). It is found that geostationary orbits go through the Earth's shadow only once per day, and only during the equinox periods (for a total of 90 eclipses) with varing eclipse times up to 72 min per day (Borthomieu, 2014), which results in almost continuous solar illumination. However, in specific circumstances, other orbits may be better suited, for example, Proctor finds that high latitude locations on Earth create inefficiencies in the power beam from satellites in geosynchronous orbit, preferring in these situations to use a Molniya elliptical orbit, and using geosynchronous orbits for locations closer to the equator (Proctor *et al.*, n.d.). Geosynchronous laplace plane (GLP) orbits can also hold benefits over traditional geostationary orbits, including resilience to perturbation (resulting in minimal or no station-keeping propellant requirements) but would require continuous beam steering (Cash, 2019).

Research into Low-Earth Orbits (LEO) indicates that LEO is a poor choice of orbit, as it results in minimal rectenna contact time and eclipses every 90 minutes (Cash, 2019), in addition to this, a stronger gravitational pull would require larger quantitiaties of propellant for station keeping (Gosavi *et al.*, 2021); despite this, LEO could be a viable choice for SBSP technology demonstrations, as Earth-to-LEO costs represent a fraction of Earth-to-GEO (Mankins, 2012).

Orbit Selection

In this literature review, Earth-to-Orbit launches primarily refer to Earth-to-LEO launches, as a variety of in-space transportation methods exist to transport the satellites from LEO-to-GEO and will be reviewed in the following section. Historically, the greatest limitation to the implementation of space-based solar power has been launch costs, making the mass of the system the most important parameter of any design. Several studies concluded that to make SBSP feasible, launch costs on the order of \$400 / kg needed to be achieved; with NASA's Highly Reusable Space Transport (HRST) study aiming to achieve direct recurring costs under \$400 / kg (Olds, 1998), Mankins' Fresh Look paper stating \$200 - \$400 per kg was necessary (Mankins, 1997), and Zapata (1999) analysing spaceport operations on the basis of launch costs of \$400 / kg. Since 2010, space launch costs have seen large reductions, with the average launch cost between 1970 and 2000 of \$18, 500 / kg falling down to \$2, 700 with SpaceX's Falcon 9, and is currently around \$1, 400 / kg with the Falcon Heavy (Jones, 2018); other sources estimate the Falcon 9 launch to be marginally higher at \$3, 000 / kg (Phen, 2022) or lower at \$2, 321 / kg (Jain & Trost, n.d.). Despite this reduction, there is a trend of rocket launch systems decreasing in payload capacity, creating a lack of heavy-lift vehicles (Jain & Trost, n.d.) which could result in potential launch issues for larger satellites, and must be considered when designing SBSP projects.

However, new launch vehicles are currently being developed too, with Virgin Galactic developing horizontal launch systems for around \$24, 000 / kg (Field, 2021) which aim to reduce costs by eliminating the need to launch the rocket from the ground and instead carry it to altitude on board a specially-fitted plane. With this idea of avoiding early use of rocket engines, a company called "SpinLaunch" has designed a slingshot-like launcher which attaches rockets to a spinning arm and propels it into space, where the rocket is then ignited once its almost in orbit, NASA is currently collaborating with this company (Goodyer, 2022). These trends signal further reductions in the cost to launch rockets, however it may be some time before the \$400 / kg is reached.

In-orbit transportation

As stated above, Earth-to-LEO is more cost-effective than Earth-to-GEO transport, however, the preferred orbit for SBSP designs is usually geosynchronous, hence, in-orbit transportation from LEO-to-GEO is necessary. Two main concepts have been developed, an orbit transfer vehicle tug that delivers the satellite from LEO to GEO, and then returns to LEO to repeat its mission (Bozek & Oleson, 1993) and propulsion systems added directly to the satellites (Oleson, 1999): both rely on electric propulsion but have fundamental differences. The electric tug detailed by Bozek (1993) relies on Space Laser Energy (SELENE) technology, which is comprised of several Earth-based laser sites which beam laser power through the atmosphere to photovoltaic cells on a tug which converts the laser power into usable electric power. It was found that a tug with laser electric propulsion, augmented with solar electric propulsion could transport 2500-kg satellites from a 500-km LEO to GEO in 65 days, and would take 37 days to return to LEO; this was modelled with four Earth sites and it was determined that a benefit / cost ratio of 2.7 could be achieved in comparison to a purely chemical mission to GEO (Bozek & Oleson, 1993). Although this result was promising, Olsen (1999) showed that Hall thrusters would provide the optimum balance in terms of launches and ground to GEO delivery time. Building upon the "SolarTower" design for SBSP, using a 20 ton mass, Hall thrusters provided shorter transport times of 153 days from LEO-to-GEO and offered station keeping abilities which make it a more optimal solution than tugs (Oleson, 1999).

Solar power collection methods

Solar power conversion methods which convert solar energy into electricity can be classified broadly into two groups: those who use passive cooling and those who necessitate active cooling. Examples of passive cooling are: silicon planar and gallium arsenide concentrators; and active cooling examples are: thermophotovoltaic conversion, Brayton, Rankine and Stirling cycle (S.R.A., 1985). Although these methods were all studied in a paper by Space Research Associates, this paper aimed to investigate space-based solar power built from lunar resources where more constraints were placed on material choices, neccesitating a larger number of options to consider; with this in mind, all current state-of-the-art SBSP designs use passive cooling photovoltaic (PV) cell arrays. Specifically, the distributed SBSP concept by McLinko (2010) uses Copper Indium Gallium Selenide (CIGS) solar cells which are thin-films, providing 19.5% efficiency; CASSIOPeiA (2019) uses millimetre-scale h-CPV (high concentration photovoltaics) providing up to 40% efficiency and SPS-Alpha (2012) uses high efficiency multi-bandgap PV cells. There is also on-going research to increase the efficiency of these PV cells with new technologies emerging (Vedda & Jones, 2020):

- Flexible thin PV film which is optimized for low mass and low cost - high-efficiency, multi-junction PV which have achieved 39% efficiency.
- Quantum dots which are a new technology, with current efficiency of 16.6% but have a theoretical limit of 66%.
- Perovskite solar cells, invented in 2012, and cost less to fabricate than silicon PV cells.

Despite these advances, solar cell degradation remains a key concern impacting cell choice. CIGS cells, such as those used in the distributed satellite design are some of the most radiation-hard solar cell materials, meaning the fluence where their efficiency is reduced by 50% is an order of magnitude higher than it is for other three-junction cell designs (Johnson *et al.*, 2009), however, their beginning of life efficiencies are much lower.

Power transmission methods

The two main methods of power transmission are laser-based and microwave-based. Laser-based transmission is also known as “direct solar pumping laser power generation”, however, research into this has shown that it is not optimal for transmitting power from satellites down to Earth for several reasons: the efficiencies and power levels obtained are very low due to difficulty in concentrating enough sunlight to achieve the lasing threshold (Winston *et al.*, 2005), and lasers are affected by weather and clouds which can introduce several dB of attenuation (Johnson *et al.*, 2009); this finding is echoed by multiple other sources such as Cash (2019) who claims that laser SPS suffers the same weather dependency as terrestrial solar. The main advantage that laser-based transmission offers is that it allows the transmitting antennas to be made smaller (Johnson *et al.*, 2009), however, in practice this is not seen as sufficient enough and all SBSP designs use microwave transmission between the satellites and Earth. Nonetheless, that is not to say that laser transmission is useless, as it can be used effectively to transmit power in space where there is no atmospheric interference (Vedda & Jones, 2020), for example, in satellite-to-satellite transmission; this is what is planned by the National Space Development Agency of Japan, which employs a concept of distributed satellites collecting energy and beaming it via laser to a main satellite, which itself beams the energy to Earth via a microwave transmission (Tandle, 2019).

Assembly scenarios

Assembly of SBSP designs refers to the in-space deployment and assembly operations which transform the satellite payload into its final fully-configured form. Assembly is inherently tied to specific SBSP designs, however there are several key technologies and ideas which have been developed.

Most SBSP concepts envisage autonomous assembly by robots, specifically Frazer-Nash (2021) details that assembly should be undertaken in Medium Earth Orbit (MEO) to avoid the risk of space-debris in LEO, this would also avoid radiation from the Van Allen belt; the system would be placed into MEO by an in-orbit transportation vehicle detailed above, and once assembly is completed, be moved again into its final orbit. The robot assemblers could be free-flying, but designs such as CASSIOPeiA (2019) and even older designs such as the "SunTower" and "SolarDisc" (Mankins, 1997) envisage assembly to be completed by mechanical systems inherent to the structure, although the wireless power transmission technology inherent to SBSP designs could also power a cluster of robots which could perform assembly or maintenance tasks (Cash, 2019).

Lunar resources exploitation

With the Moon possessing a fraction of Earth's gravity, deploying space assets using lunar resources has been attractive since the start of space exploration. Several key studies have investigated the possibility of exploiting lunar resources to make space-based solar power a reality, including "Solar Power Satellite Built of Lunar Resources" by Space Research Associates (1985) and "Lunar-Based Self-Replicating Solar Factory" by Lewis-Weber (2016); with both studies concluding that using lunar resources can offer significant cost savings in comparison to traditional space-based solar power implementations if technological hurdles can be overcome.

Space Research Associates (1985) found that silicon planar could be used as an efficient lunar-based solar power conversion system, with aluminium used for the structure as well as acting as a major material in most of the other components such as the microwave lens, waveguides, and main buses. The solar replicating factor conceptualized by Lewis-Weber (2016) includes a mass driver, with a cluster of robots exploiting the lunar surface and creating the necessary components for space-based solar power.

2.4. Modelling Methodology

Solar power generation calculations

Calculating the solar power generation of potential SBSP can be split into two main categories based on their granularity.

The first method is high-level and relies on identifying incident solar radiation, and determining the overall efficiency of the system. The solar constant flux density measures the intensity of the sunlight hitting the satellite and can be taken as 1367 W / m^2 at orbits around Earth (Etchells, 2019), it typically varies between 1365 and 1367 W / m^2 annually

(Gorev *et al.*, 2019); assuming the satellite is in geosynchronous orbit, this intensity is applied near-continuously and can be factored by the solar array size and overall system efficiency to compute solar power generation values. This method is rudimentary but can be used to determine average values of solar power generation over a longer-term time horizon (eg. several years) and is generally used for studies of SBSP designs, for example for that of CASSIOPeiA (Cash, 2019) or when comparing SBSP to other energy sources (Smitherman, n.d.); and can be augmented by factoring in the exact amount of time the satellite would spend in sunlight at different orbits.

The second method is much more granular and involves modelling the system at a lower-level, including volumetric analysis of the satellite, size of the photoconverters and location and more to determine solar insolation; electric power is calculated at each time-step for specific angles and irradiances (Gorev *et al.*, 2019). A similar concept is proposed by Etchells (2019) with various orbit models. Both these granular models were written with an application to CubeSats and not SBSP designs, although the theory should not change.

Solar power degradation

The above calculations did not take into account degradation of solar cells which are a known issue in space operations, and should be taken into consideration to generate the most reliable power generation outputs.

Solar cell degradation is factored into these methods by two means: an inherent degradation factor, and a lifetime degradation factor (Etchells, 2019). The inherent degradation factor reflects inefficiencies in reported conversion efficiencies between a single solar cell and a fully-integrated solar panel, a typical value is 77% (Etchells, 2019). Lifetime degradation accounts for the gradual decline in solar cell efficiency throughout its operational lifetime. Lifetime degradation factors are known to solar cell manufacturers, for example, in problem-sets at MIT, Si PV cell degradation is taken to be 3.75% per year and GaAs PV cell degradation is taken to be 2.75% (Nadir, 2003). However, more advanced studies have looked at real-life data of solar PV degradation and reported results, for example, solar panels on the ISS were found to have up to 0.45% measured degradation per year (Kerslake & Gustasfon, 2003). Furthermore, models such as SAVANT have been established to predict solar cell degradation in space radiation environments (Messenger *et al.*, 2000).

3. Methodology

Assessing the energy generation potential of space-based solar power concepts entailed a simulation-based approach. At a high level, the method takes input parameters of the system (orbit, the satellite, ground station...) and returns the computed energy generated over the specified time window.

The development of the model led to two classes of solutions: class I aims to calculate the power generated by SBSP concepts as found in the literature, this led to a general model which can be applied to any SBSP system, relying only on basic information as traditionally covered in such papers; class II developed the power model from a more fundamental approach, which assumes a simplified model of an SBSP implementation, in order to conduct sensitivity analyses and examine the impact of architectural choices on the system.

The two classes differ by their power equation, but contain a large amount of overlap as they both address the same problem. Specifically, as figure 1 shows,

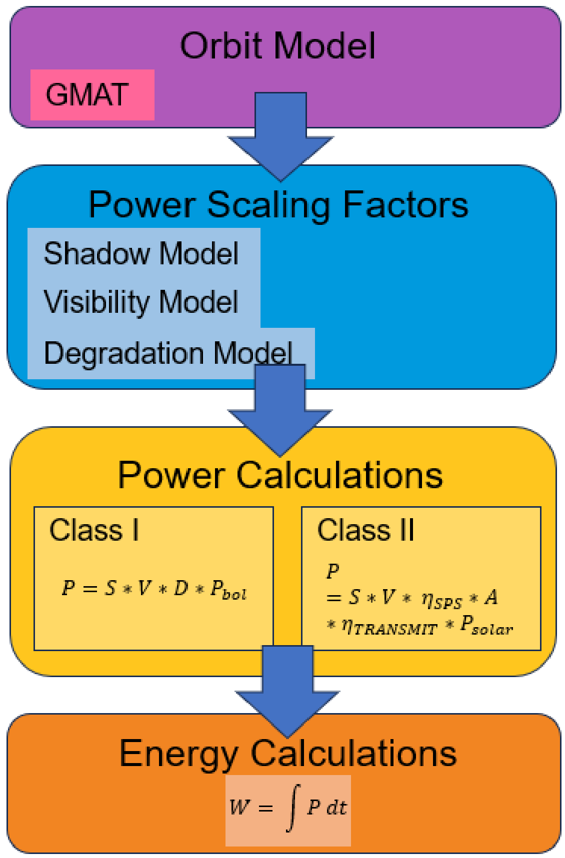

Figure 1: Flowchart showing the interlinking components of the methodology.

both classes use an orbital model to simulate the relevant bodies (Earth, Sun and satellite) in space and time, which is then combined with shadow, visibility and degradation models; the differences subsequently appear in their specific power computations; both classes then share the final step converting power to energy. The approach combines the orbital results from the GMAT application with Python and Matlab code implementing the other models; Python was used because of its vast number of libraries, and the ability to develop open-source packages.

3.1. Orbital Simulations

The first and most fundamental step when simulating space-based solar power systems is to model the positions of the relevant celestial bodies and satellites; this was achieved with an orbit model. This stage is especially important to the overall process, as the information it produces is the basis upon which subsequent models (shadow, visibility...) are applied.

The goal of the orbital simulation was to take parameters describing the satellite orbit, as well as parameters relating to the satellite itself, and output positions of the Earth, Sun and satellite for each timestep of the simulation duration.

In this research, the General Mission Analysis Tool (GMAT) was used as the orbit model. It is an open-source software application developed by a team at N.A.S.A. and private industry and is designed for space mission design (N.A.S.A, n.d.), this includes functionality for modelling satellites, as well as visualisations of ground tracks, and satellite orbits in three dimensions. GMAT was chosen as it is free, widely documented and extensively tested for reliability and accuracy of results.

When placing satellites in space, several orbit types exist. Depending upon the altitude above earth, an orbit can be a Low Earth Orbit (LEO), Medium Earth Orbit (MEO) or Geosynchronous Orbit (GSO); other commonly found orbit types are polar and Sun-synchronous orbits (SSO), and transfer orbits. Two orbit types are examined in this paper: Geostationary orbits (GEO) are a type of Geosynchronous orbit appearing to be "stationary" above a point on Earth, and are utilized in Class I; low earth orbits are also used in class II.

Simple Orbits

Three stages are needed when simulating simple orbits in GMAT:

1. Configuration of the spacecraft, its epoch and orbital elements: this involves setting the mass of the satellite, the epoch of the simulation, and the orbital elements, as listed in table 1.
2. Configuration of the propagator: this involves setting the integrator and the force model.
3. Configuration of the propagation duration: this involves setting the stopping conditions for the propagator.

Table 1: Description of Keplerian orbital parameters and their conditions of undefinability.

Orbital Parameter	Undefined Condition
a - semi-major axis	N/A
e - eccentricity	N/A
i - inclination	N/A
Ω - Right ascension of the ascending node (RAAN)	$i = 0° or 180°$
ω - Argument of periapsis	$i = 0° or 180°$ or $e = 0$
ν - True anomaly	$e = 0$

The orbital parameters and coordinate system chosen for this analysis should be considered. The orbital elements GMAT uses can be set in a variety of forms and depend on the chosen coordinate system; those detailed in table 1 are Keplerian orbital elements and are the chosen form for this study. Additionally, this study uses the GMAT default coordinate system "EarthMJ2000Eq" when setting the orbital elements, but uses the Earth-centred Earth-fixed coordinate system when reporting the positions of the Earth, Sun and satellite. Details of these coordinate systems are available in appendix 7.1.

Station-Keeping

Whilst it is possible to simulate the trajectory of satellites with a simple orbit as outlined above, a phenomenon named "orbital decay" would become apparent as the duration of the simulation increases. All satellites in orbit are subject to perturbing forces which can destabilise them from their initial orbit, this leads the notion of "orbital lifetime": the amount of time a satellite has before re-entering the Earth's atmosphere. In particular, satellites at altitudes of 200km (in LEO) typically have an orbital lifetime of several hours to 1 day (SpaceAcademy, n.d.). Counteracting orbital decay is achieved by manoeuvring the satellite with thrusters, and is called station-keeping.

For a satellite in LEO, station-keeping is used to counter the effects of atmospheric drag, causing the satellite to lose altitude. GMAT possesses a script for LEO station keeping which was configured to match the desired simulation duration and temporal resolution, details are available in 7.2. The algorithm uses impulsive burns which are activated when the satellite's position is outside the bounds of an imaginary box, at this point, burns are computed which would place the satellite back in position. This algorithm is not typical of those found onboard real-world satellites where precisely computed finite burns would be activated at scheduled intervals. However, for the purposes for this study, the orbital model simply needed to provide a feasible orbit and did not need to involve high-fidelity recreations of real-world orbits.

For a satellite in geostationary orbit (GEO), the effects of atmospheric drag are negligible, instead two principle effects create the need for station-keeping:

- The combined gravitational forces of the Sun and the Moon on the satellite cause the orbital inclination to increase by almost one degree per year, necessitating North-South station-keeping manoeuvres which bring the satellite to within 0.05° of its original inclination (Darling, n.d.).
- The bulge of the Earth causes a longitudinal drift which is compensated by East-West station keeping-maneuvers to keep the satellite within 0.05° of its assigned longitude (Darling, n.d.).

In contrast to LEO station-keeping, GMAT does not provide a script which addresses GEO station-keeping. Additionally, no reproducible sources were found in the literature about specific algorithms for this task; fortunately, a GEO station-keeping tutorial was found in the documentation of Ansys STK (Ansys, n.d.), a similar software to GMAT. This was heavily adapted to work with impulsive burns in GMAT and only includes provisions for East-West station keeping for two main reasons: a significant increase in computing time due to the calculation of double the number of impulsive burns, and the inclination was not found to increase at such a rate as to impact the orbit significantly, especially with the longitude being controlled by the East-West station keeping. The implementation is detailed in algorithm 1.

Algorithm 1 Geosynchronous orbit: East-West Station Keeping

```
while ElapsedDays < SimulationDuration do
    Propagate one step
    if Longitude <|> Tol then
        Propagate to apoapsis
        while AcheivedLongitude <|> Tol do
            Vary ThrusterBurn
            Apply ThrusterBurn
            Propagate to ascending node
            Acheive longitude
        end while
    end if
end while
```

Model validation

Although the algorithms behind GMAT have been extensively tested, it was possible to validate certain results, notably that the orbital period reported by GMAT matched the theory. According to Kepler's Third Law (harmonic law), the ratio of the cube of the semi-major axis to the square of the orbital period is a constant (Vanderbilt, n.d.). This equates to equation 1:

$$\frac{a^3}{p^2} = \frac{G(M_1 + M_2)}{4\pi^2}, \tag{1}$$

which can be rearranged and simplified to make p the target, leading to equation 2:

$$p = 2\pi\sqrt{\frac{a^3}{G(M_1 + M_2)}}, \tag{2}$$

Equation 2 was then compared to the results reported by GMAT for the same semi-major axis a and satellite mass M_1. G is the gravitational constant ($6.67430 * 10^{-11}$ Nm^2/kg^2) and M_2 is the mass of the Earth.

3.2. Power Scaling Factors

3.2.1. Shadow Model

Solar panels need sunlight to produce electricity, therefore, a model determining the amount of sunlight a satellite receives was developed. The model's objective was to predict the level of solar shading a satellite experienced along its orbit, but was not concerned with identifying whether some parts of the satellite were in the shade and others were in sunlight, or whether some parts of the satellite were blocking the sunlight for other parts.

At a high level, the model receives as input the satellite, Sun and Earth positions from the orbital simulations, and outputs the level of sunlight being received by the satellite, in the form a number between 0 (no illumination) and 1 (full illumination). Several shadow model derivations exist in the literature, these can be classed into two main types: spherical Earth cylindrical model (CYM) (figure 2) and the more complex spherical Earth conical model (SECM) (figure 3). It should be noted that the shadow models used in this study considered occultations where the Earth casts a shadow on the satellite, and ignores those where the Moon casts a shadow on the satellite; these were neglected because they occur less frequently and in a "random" manner (Montenbruck & Gill, 2001).

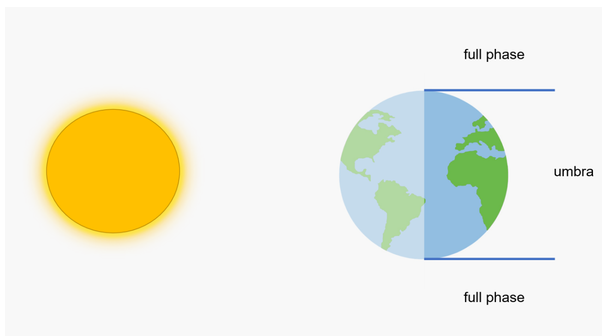

Figure 2: Spherical Earth cylindrical model (CYM) diagram.

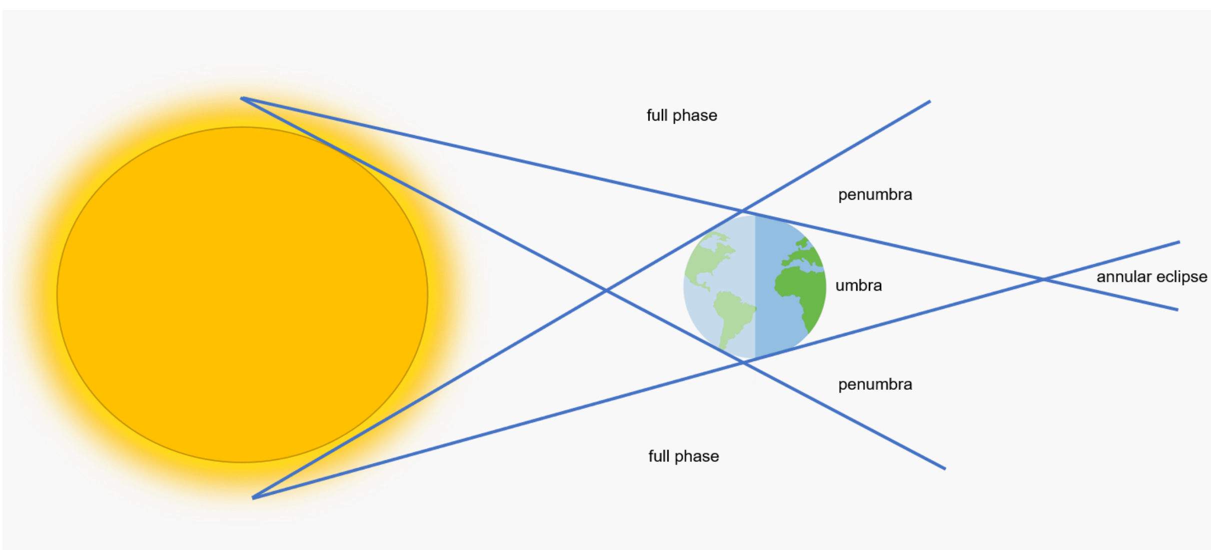

Figure 3: Spherical Earth conical model (SECM).

An implementation of an SECM model was taken from the book "Satellite Orbits: Models, Methods, Applications" by Montenbruck (2001), and adapted for Earth-orbiting satellites. The model is computed using the angular separation and diameters of the Sun and the Earth, with figure 4 showing the overall geometry where R_{sun} is the radius of the Sun, R_B is the radius of the occulting body (the Earth), $\boldsymbol{r_{sun}}$ is the vector from the central body (Earth) to the Sun and $\boldsymbol{r}$ is the vector from the central body (Earth) to the satellite.

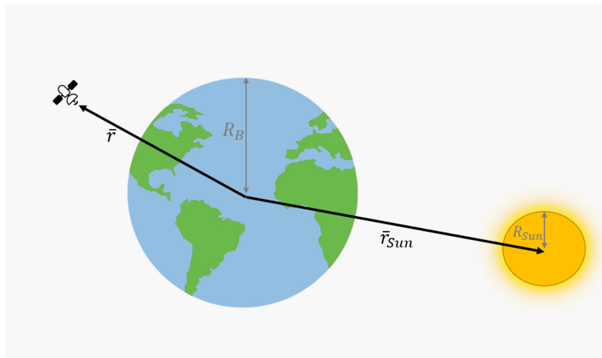

Figure 4: Montenbruck's shadow model geometry.

Due to the small apparent diameter of the Sun, it is sufficient to model the occultation by overlapping circular disks (Montenbruck & Gill, 2001), figure 5 illustrates this.

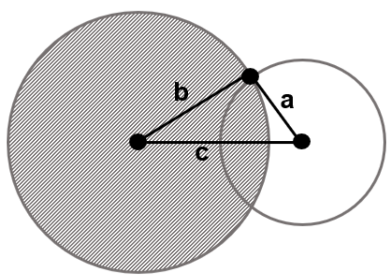

Figure 5: Overlapping disk geometry from the Montenbruck shadow model.

From Montenbruck (2001), the apparent radius of the occulted body (the Sun) is:

$$a = arcsin\frac{R_{sun}}{||\boldsymbol{r_{sun}} - \boldsymbol{r}||}, \tag{3}$$

the apparent radius of the occulting body is:

$$b = arcsin\frac{R_B}{||\boldsymbol{r}||}, \tag{4}$$

with the apparent separation of the centres of both bodies being:

$$c = arcos\frac{-\boldsymbol{r_{sun}}^T(\boldsymbol{r_{sun}} - \boldsymbol{r})}{||\boldsymbol{r}|| \cdot ||\boldsymbol{r_{sun}} - \boldsymbol{r}||} \tag{5}$$

According to Montenbruck (2001), if $c >= a + b$ then no occultation takes place and S = 1 (full sunlight regime). On the other hand, if $c < b - a$ occultation is total and S = 0 (umbral regime). Finally, if $|a - b| < c < a + b$, then the satellite is in the penumbra and the occulted area is given by equation 6:

$$A = a^2 arcos\frac{x}{a} + b^2 arcos\frac{c - x}{b} - cy, \tag{6}$$

where $x = \frac{c^2+a^2-b^2}{2c}$ and $y = \sqrt{a^2 - x^2}$. The fraction of sunlight is then given by equation 7 (Montenbruck & Gill, 2001):

$$s = 1 - \frac{A}{\pi a^2} \tag{7}$$

Model Validation To verify the accuracy of the algorithm, the results were compared with GMAT by verifying that the transitions from one regime to another have the same epochs.

3.2.2. Visibility Model

Contrary to satellite power models which only need to track the power a satellite can generate, space-based solar power relies on being able to transmit that power to a ground station on Earth, to account for this, a visibility model was used. The model's purpose was to identify periods when no line of sight existed between the satellite and the ground station, when no power could be transmitted.

Despite the need for such a model, no suitable sources were found in the literature, hence it was derived from first principles. The model receives as input the Earth, satellite and ground station positions and returns a binary result, 0 (no line of sight) or 1 (line of sight exists). The model geometry, simplified to two dimensions is shown in figure 6.

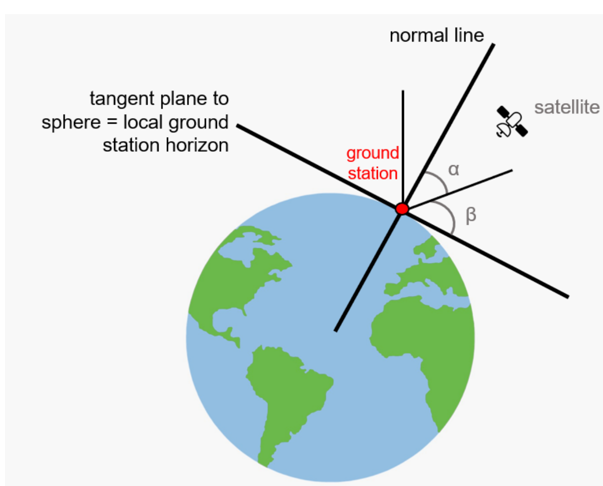

Figure 6: Illustration showing geometry of the visibility model in two dimensions.

Step 1: Locating the ground station

When describing locations on Earth, it is common to use geodetic coordinates of longitude (-180° to +180°) and latitude (-90° to +90°). However, the coordinate systems used up until this point were EarthMJ2000Eq to set the Keplerian orbital elements, as well as Earth-centred Earth-fixed (ECEF) for the positions of the Earth, Sun and satellite, therefore a conversion between ECEF and geodetic was needed. According to Clynch (2002), given latitude ϕ, longitude λ, and geoid height h, then the coordinates in ECEF are:

$$x = (R_N + h) * cos(\phi) * cos(\lambda), \tag{8}$$

$$y = (R_N + h) * cos(\phi) * sin(\lambda), \tag{9}$$

$$z = ([1 - e^2]R_N + h) * sin(\phi), \tag{10}$$

where $R_N = \frac{a}{\sqrt{1-e^2 sin^2\phi}}$ and $e^2 = 1 - \frac{c^2}{a^2}$, with a the equatorial radius (6378 km) and c the polar radius (6357 km). It should be noted that the geoid height is different to what is typically thought of as height (which is mean sea level height or altitude), to convert between the two, a geoid model with a lookup table for specific locations is needed, however, for our purposes, the height of the ground station is of no physical significance, and the difference between the two is minimal, hence altitude was used instead. This is illustrated in figure 7.

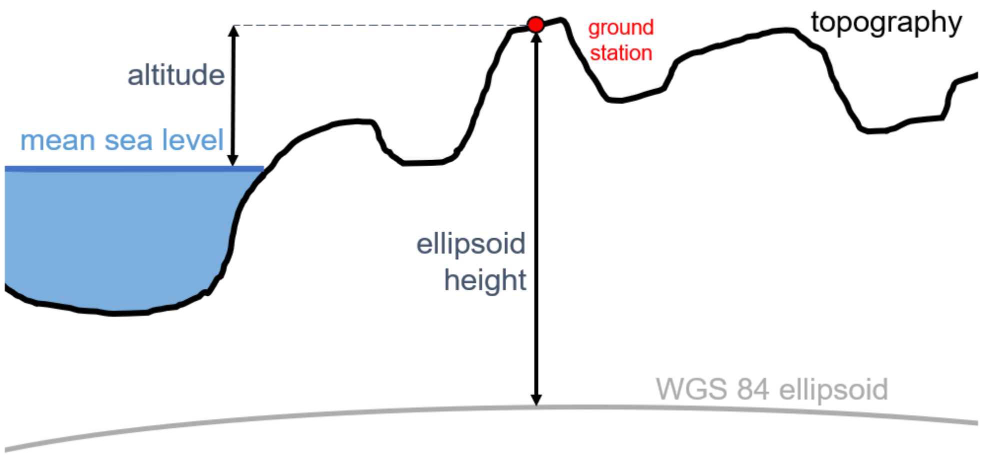

Figure 7: Illustration showing the difference between altitude and ellipsoidal height.

Step 2: Finding the horizon

Representing the Earth as the WGS 84 ellipsoid, then the formula for the surface in Cartesian coordinates is given by equation 11:

$$\frac{x^2}{a^2} + \frac{y^2}{b^2} + \frac{z^2}{c^2} = 1 \tag{11}$$

where $a = b$ is the semi-major axis or equatorial radius, and c and is the semi-minor axis or polar radius. The ground station was assumed to be small compared to the size of the Earth, and the Earth to be locally flat over this small area, then the horizon for a location could be interpreted as the tangent plane to the ellipsoid at that point as in equation 12, for a surface $f(x, y, z) = k$ at a point x_0, y_0, z_0 representing the coordinates of the ground station:

$$f_x(x_0, y_0, z_0)(x - x_0) + f_y(x_0, y_0, z_0)(y - y_0) + f_z(x_0, y_0, z_0)(z - z_0) = 0 \tag{12}$$

where f_x, f_y, f_z are components of the gradient vector $\nabla = \langle f_x, f_y, f_z \rangle$.

Step 3: Locating the centre of the viewing cone

The line emanating from the Earth's centre to space passing by the ground station is the normal line at that location and could be interpreted as the centre of the viewing cone. This is given by 13:

$$\boldsymbol{r}(t) = \langle x_0, y_0, z_0 \rangle + t \cdot \nabla f(x_0, y_0, z_0) \tag{13}$$

Step 4: Computing relative positions For clarity, let the following points be defined which are described in table 2.

Table 2: Description of the important points of the visibility model.

Point	Definition
A	Ground Station
B	Along the normal line, at a height from A
C	Satellite
D	Projection of C onto the normal line

Point B is found using equation 13 with $t = 1$; any value for t can be used as the vector $\vec{AB}$ is only needed for its direction which is then used to find point D. D is the vector projection of $\vec{AC}$ on $\vec{AB}$ added to point A, as given by equation 14:

$$D = A(x, y, z) + proj_v u \Rightarrow A(x, y, z) + (\frac{u \cdot v}{||v||^2}) \cdot v, \tag{14}$$

where u is $\vec{AB}$ and v is $\vec{AC}$. The height of the satellite above the ground station is the length of the projection, as in equation 15:

$$AC = comp_v(u) = ||proj_v u|| = \frac{u \cdot v}{||v||} \tag{15}$$

Step 5: Defining the cone of visibility

The minimum elevation angle β_{view} shown in figure 6 takes into account the angle from the horizon which cannot be viewed because of topographical features such as mountain ranges. This can be converted into the viewing angle α_{view} with the relation shown in the figure. Thus, the radius of the cone of visibility at the height AD is:

$$R_{cone} = AD * tan(\alpha_{view}), \tag{16}$$

with the distance between the satellite and point D being governed by:

$$CD = |AC - AD| \tag{17}$$

Step 6: Conditional checking If $CD <= R_{cone}$ then the satellite is visible and $V = 1$, else $V = 0$.

Model Validation

To validate this algorithm, the results of the geodetic to ECEF conversion were compared with an online implementation by the Naval Postgraduate School (N.P.S, n.d.); and GMAT has a satellite access to ground station function: similarly to the shadow function, the accuracy can be validated by verifying that the transitions from one regime to another have the same epochs.

3.2.3. Degradation Model

As a result of the space environment, components of space-based solar power will degrade over time, affecting the overall efficiency of the system. A degradation model was developed to account for this.

The model accounted for degradation as a function of time, and outputted a factor between 0 (full degradation - no power generated) and 1 (no degradation - initial state); the inputs were the rate of degradation and the current timestep of the simulation.

Degradation is a result of the combined loss in efficiency of the individual components which make up the space-based solar power concepts, any model should aim to integrate all these effects, but practically this may be too complex to model. This could be formulated mathematically as a weighted average degradation factor in equation 18:

$$D = \frac{\sum_{n=1}^{n} \omega_i X_i}{\sum_{n=1}^{n} \omega_i}, \tag{18}$$

where ω_i is the proportion of energy affected by a component, and X_i is the degradation rate of a component.

This approach however has its limitations; the model quickly becomes complex and necessitates a level of understanding of the system, and forces the model to become less general as a result. Furthermore, the question of granularity and how components should be accounted for arises. Finally, modelling of individual components could be complex or inaccurate due to a lack of research for particular components. For these reasons, this method was not chosen in this study.

A simpler model was considered, consisting of a single parameter: the rate of degradation of the solar panels. This model has distinct advantages over the latter; an abundance of research exists for modelling the degradation of solar panels in space environments, and space solar cell manufacturers detail degradation rates on their datasheets.

A limitation of this model is the fact that all other degradation of the system is ignored, but this is not as significant as expected because their impact on the energy losses of the system are minimal. In MR-SPS's paper (Hou *et al.*, 2021), a breakdown of the efficiency of major components reveals that the solar cell is the first component in the energy loss chain, with an efficiency of 0.29,; the total efficiency of the system is reported as 0.138. This means that by only including the solar panel losses around 85% of the degradation is accounted for. Incorporating the effects of time, this becomes:

$$D(k,t) = e^{-kt}, \tag{19}$$

where k is the daily degradation rate and t is the timestep of the simulation, in days.

3.3. Power Calculations

3.3.1. Class I

As shown in figure 1, the power of SBSP systems for Class I is given by equation 20:

$$P = S * V * D * P_{BOL} \tag{20}$$

P_{BOL}

This value is the power (in Watts) that the system can generate at any one time at the start of its life, it is not computed but is instead taken from the literature.

State-of-the-art SBSP concepts today have complicated geometrical shapes and architectures which would necessitate complex modelling to calculate power generation; but papers invariably detail P_{bol}, allowing for a simple energy model as in this paper. In fact, often SBSP designs base themselves on this value, and aim to design a concept which can produce a specific wattage. When taking these values from the research, this paper has made several assumptions which are not always clearly detailed in the relevant SBSP study:

- The listed power is the power at the beginning of life of the concept, and does not include degradation factors; it is also not a power which is averaged over the duration of the mission lifetime: The power is not time-averaged.
- The listed power takes account for the geometry of the shape, and is the power that can be generated at any one time, regardless of orientation: the power is spatially-averaged.
- The listed power is the power of the entire system from solar collection to reception and conversion at the ground station.
- Solar radiation is assumed to be constant at a value of 1367 W/m^2, the Earth average solar radiation at 1 astronomical unit (AU) distance (W.M.O, 1986).

3.3.2. Class II

Class II was designed as a sensitivity analysis, and hence has a different approach to calculating power output. This class of solutions analysed how orbit choice, degradation and solar cell choice affect the overall energy production of the system; because the solar cell is now a design choice, it is no longer possible to compute the power using P_{bol} as in class I.

To do such an analysis, this class assumed a simplified and idealised model of space-based solar power, where the satellite is a circular disk with an area of 1 km^2, which is constantly sun-pointing so that its entire area is in sunlight when not in the shadow; it also equipped with microwave power transmission capabilities with an efficiency of 0.5, typical of SBSP. With such a system, a thermo-electrical model of the solar panels in space was possible, but had limitations: a lack of reproducible research, and unreliable results due to a lack of real-world data. A different approach was chosen where the power was calculated as in equation 21:

$$P = S * V * \eta_{SPS} * A * \eta_{TRANSMIT} * P_{solar} \tag{21}$$

Efficiency Model

The total power produced by a solar panel depends on its efficiency, often this is thought of as a single value but a temperature dependence exists. The efficiency variation with temperature is generally non-linear, but in the range from -100 degrees to a few hundred degrees C, efficiency can be accurately modelled as a linear function (Landis, 1994).

Evans and Florschuetz (1977) state the temperature dependent efficiency is given by equation 22:

$$\eta = \eta_r[1 - \beta_r(T_c - T_r)], \tag{22}$$

where the efficiency η depends on η_r, the cell efficiency at reference temperature T_r, T_c, the temperature for which the efficiency is computed and β_r, the fractional decrease of cell efficiency per unit temperature increase. According to (Landis, 1994), the fractional change in efficiency per degree Celsius is:

$$\frac{1}{\eta}\frac{d\eta}{dT} = \frac{1}{V_{oc}}\frac{dV_{oc}}{dT} + \frac{1}{J_{sc}}\frac{dJ_{sc}}{dT} + \frac{1}{FF}\frac{dFF}{dT}, \tag{23}$$

where V_{oc} is the open circuit voltage, J_{sc} is the short-circuit current density and FF is the fill factor; details of these and more are available in appendix 7.3. It should be noted that Landis (1994) states the fractional change whereas Evans and Florshuetz (1977) state the fractional decrease, meaning a negative change will be a positive value of fractional decrease.

Space solar cell manufacturers datasheets include nominal values for V_{oc}, J_{sc}, as well as V_{mp}, J_{mp} and their respective rates of change, however, information relating to the fill factor or its derivative are seldom present and must be found from electrical circuit theory. Wilcox (2013) derives the fill factor relative temperature coefficient as in equation 24:

$$\frac{1}{FF}\frac{dFF}{dT} = \frac{1}{V_{mp}}\frac{dV_{mp}}{dT} + \frac{1}{J_{mp}}\frac{dJ_{mp}}{dT} - \frac{1}{J_{sc}}\frac{dJ_{sc}}{dT} - \frac{1}{V_{oc}}\frac{dV_{oc}}{dT} \tag{24}$$

Thermal Model

With the temperature-dependent efficiency determined, it was necessary to find the temperature of the solar cell. Many computational models exist however, these were found to be outside the scope of this study as they provide a level of detail which is unnecessary given the idealised implementation this paper considers.

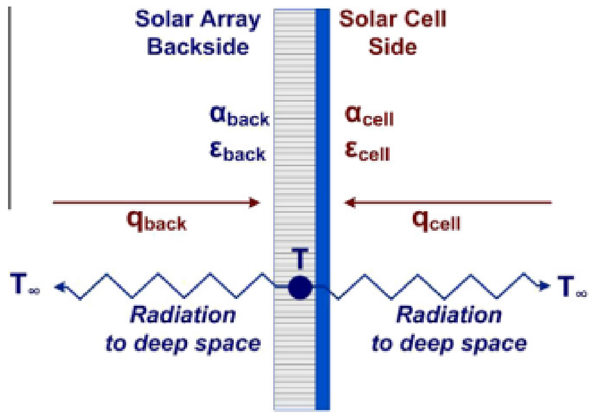

Figure 8: Kim and Han simplified temperature model, taken from Kim and Han (2010).

For a single-lumped mass only with external heating and radiation terms as in figure 8, Kim and Han (Kim & Han, 2010) state the thermal balance governing equation in 25:

$$mCp\frac{dT}{dt} = Q_{cell} + Q_{back} - \sigma\varepsilon_{cell}A(T^4 - T_\infty^4) - \sigma\varepsilon_{back}A(T^4 - T_\infty^4) = 0 \tag{25}$$

Assuming a steady-state $\frac{dT}{dt} = 0$ and the deep space condition of $T_\infty = 0$, then equation 25 simplifies so that an analytical solution exists, given by equation 26 (Kim & Han, 2010):

$$T = \sqrt[4]{\frac{\alpha_{cell}q_{solar} + \varepsilon_{back}q_{EarthIR} + \alpha_{back}\beta q_{solar}}{\sigma(\varepsilon_{cell} + \varepsilon_{back})}} \tag{26}$$

where α is the solar absorptivity, ε is the solar emittance, β is the Earth albedo (typically 0.3) (N.A.S.A, 2014), σ is the Stefan-Boltzmann constant ($5.670 * 10^-8W/m^2K^4$), q_{solar} is the solar flux (P_{solar} from above), and $q_{EarthIR}$ is the Earth's infrared flux, taken as $249W/m^2$ (Kim & Han, 2010).

P_{solar}

For an average distance of 1AU from the Sun, the Earth receives a solar flux $P_{solar} = 1367W/m^2$. In orbit however, this distance changes, influencing the value of P_{solar} according to equation 27 (Honsberg & Bowden, n.d.):

$$P_{solar} = \frac{R_{sun}^2}{D^2}H_{sun}, \tag{27}$$

where R_{sun} is the radius of the Sun in meters, D is the distance from the Sun to the satellite in meters, and H_{sun} is the power density at the Sun's surface found from the Stefan-Boltzmann blackbody equation and is $64 * 10^6[W/m^2]$

Degradation Model

Although it is reasonable to use the same degradation model as previously discussed, it is possible to directly account for using the cell datasheets which include degradation factors for the parameters discussed in the efficiency model. These are based on a target fluence at the end of the mission lifetime, but assuming a linear relationship, values during the mission lifetime can be found with the following formula as equation 28:

$$D(t) = 1 - \frac{t}{EOL}(1 - D_{EOL}), \tag{28}$$

where t is the elapsed simulation duration in days, EOL is the total duration of the simulation in days, and D_{EOL} is the end-of-life retention factor. These values were computed for each of the parameters and then substituted into the fractional change in efficiency calculations.

3.4. Energy Calculations

In order to provide results which can be used for cost-benefit analyses and more, energy is the standard unit used, as it takes into account how long power can be generated for. Energy can be related to power by its very definition: power is defined as the rate of work (or energy) $P = \frac{dW}{dt}$, leading to equation 29:

$$W = \int P dt \tag{29}$$

With a timeseries of power values, energy was found using numerical integration performed using Matlab's `trapz()` function.

4. Results and Discussion

In this section, results relating to the two classes of solution are presented. This section is split into two main sections, the first presents results from the orbital simulations, shadow, visibility and degradation models; following this, the energy generation potential of Class I and II are demonstrated.

4.1. Preliminary Results

4.1.1. Orbital Simulations

To examine and validate the orbit model, a satellite with the default GMAT characteristics in table 3 was selected.

Table 3: Chosen ballistic characteristics for GMAT simulation 1 (GEO with no station-keeping).

Ballistic Characteristic	Selected Value
Dry Mass	850 kg
Coefficient of Drag	2.2
Coefficient of Reflectivity	1.8
Drag Area	$15m^2$
SRP Area	$1m^2$

This was simulated with a geostationary orbit, whose Keplerian orbital parameters are detailed in table 4; the simulation start epoch was 1st January 2023, with a duration of 15 years, to replicate the typical mission lifetime of space solar satellites. The configuration of the propagator which computes the position of the satellite for each time-step had to be carefully selected to balance accuracy with computing speed, an initial step size of 1 hour with a maximum of 2 hours was selected, allowing the simulation to have a sufficiently high resolution whilst not taking significant computing time.

Table 4: Chosen Keplerian orbital elements for GMAT simulation 1 (GEO with no station-keeping).

Orbital Parameter	Undefined Condition
a - semi-major axis	42,164 km
e - eccentricity	0
i - inclination	0°
Ω - Right ascension of the ascending node (RAAN)	0°
ω - Argument of periapsis	0°
ν - True anomaly	0.7°

The ground track produced by the satellite is illustrated in fig 9, and shows several phenomena. Orbits degrade over time due to the action of various forces and effects; despite having an initial geostationary orbit, where the ground track should be a single point on the ground, this is not the case, and the satellite leaves a path on the map.

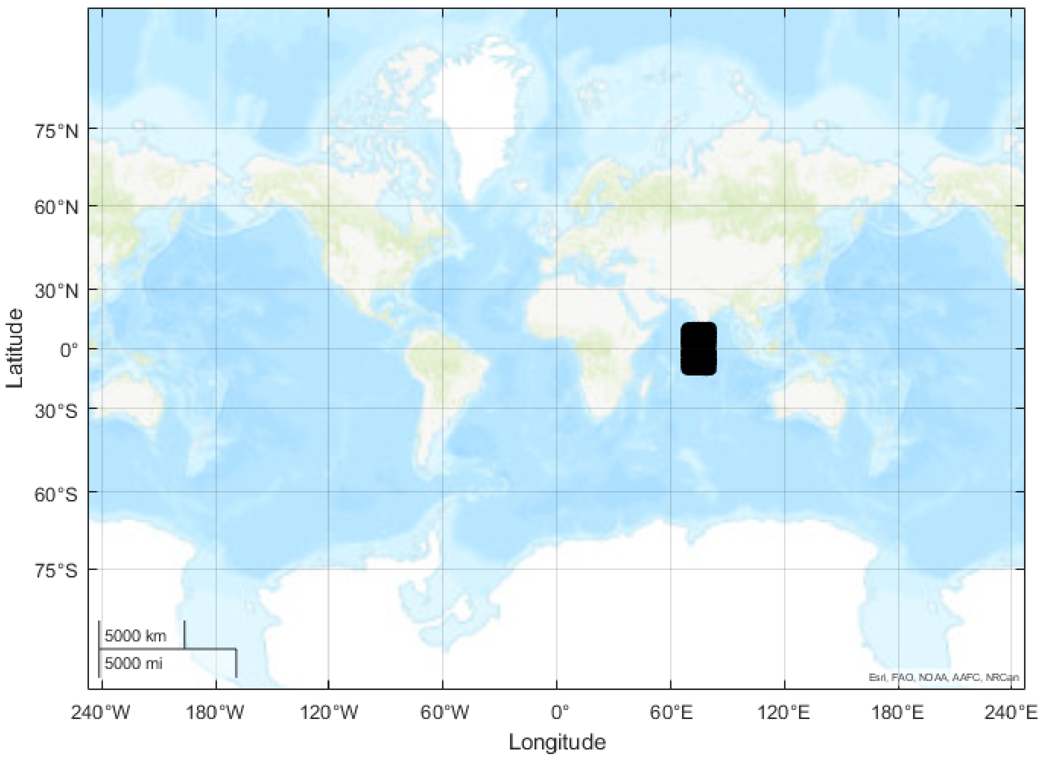

Figure 9: Satellite ground track for GMAT simulation 1 (GEO with no station-keeping).

The inclination also changes over the mission duration, as is seen in figure 10, reaching more than 10° at the end of the simulation. Furthermore, although difficult to notice from the ground track, it is possible to see the satellite's longitudinal drift due to the Earth's asymmetry in figure 11; geosynchronous orbits have 2 stable points (75°E and 105°W) (Anderson, 2015), with the satellite clearly demonstrating an oscillatory movement around this longitude; the average longitude was found to be 75.13°, very close to the point of stability.

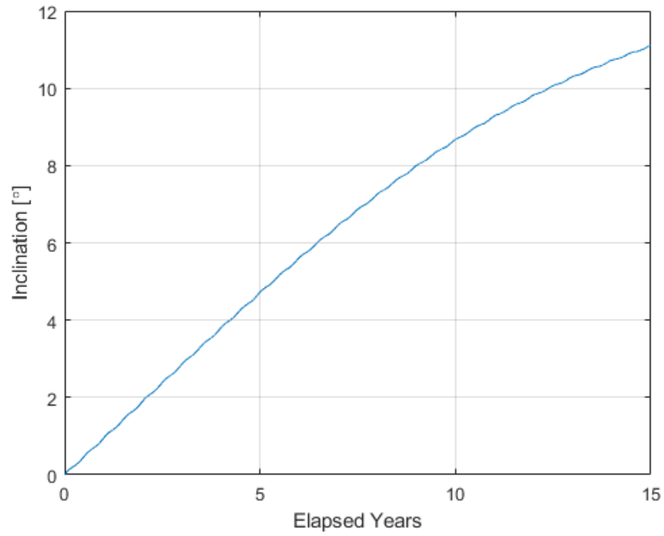

Figure 10: Orbital inclination over mission duration for GMAT simulation 1 (GEO with no station-keeping).

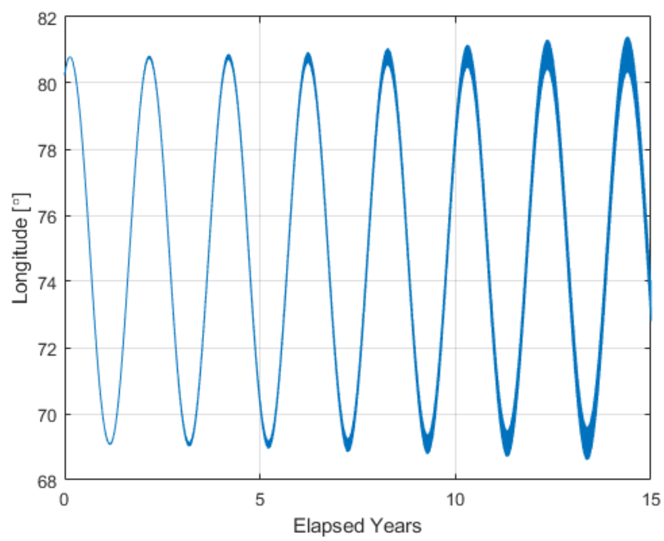

Figure 11: Satellite longitude over mission duration for GMAT simulation 1 (GEO with no station-keeping).

Station-keeping was implemented to combat orbital degradation, following the process detailed in the methodology for the same initial orbit as above; but with a propagator initial timestep of half a day, and maximum timestep of one day, in order to make the computational time feasible.

The thruster firings are shown in figure 12. The total delta-v for East-West station keeping was 212 m/s per year; as the figure indicates, large burns occur during the first year, these were neglected and the average delta-v became 137 m/s per year. However, Darling (n.d.) states typical East-West station keeping uses an annual delta-v of 2 m/s; this difference could be due to incorrectly sized impulsive burns which overcompensate forcing another burn in the opposite direction, this would seem to be indicated by the periodic nature of the burns shown in the figure.

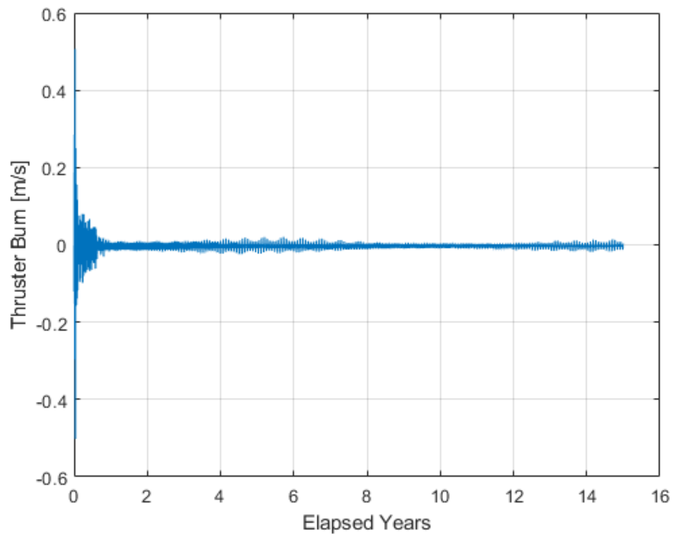

Figure 12: Satellite thruster burns for GMAT simulation 2 (GEO with station-keeping).

The ground track for this orbit, shown in fig 13, shows a different orbital regime to the previous orbit with no station keeping: there is almost no longitudinal spread, and the satellite never reaches the GEO stability point of 75°, this difference in regime can be observed by comparing the previous longitude plot with 14. This trend shows how despite the station-keeping, there are still increasing oscillations around the initial longitude; however, it was possible to verify that station-keeping was having an impact by plotting the achieved longitude after the station keeping maneuver, as is shown in figure 15.

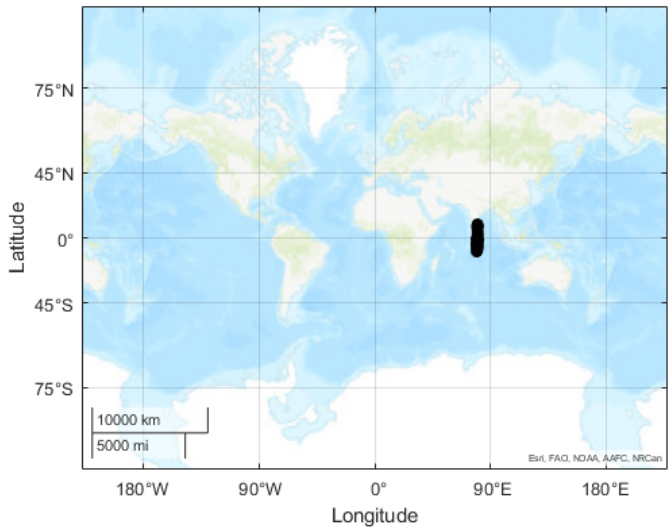

Figure 13: Satellite ground track for GMAT simulation 2 (GEO with station-keeping).

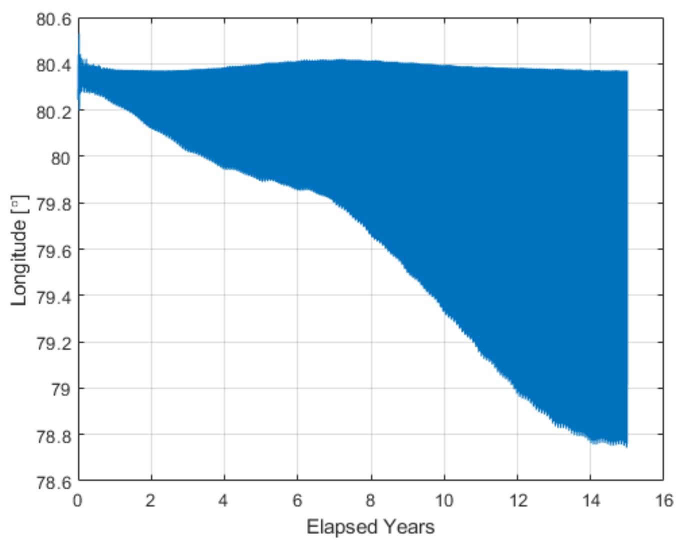

Figure 14: Satellite longitude over mission duration for GMAT simulation 2 (GEO with station-keeping).

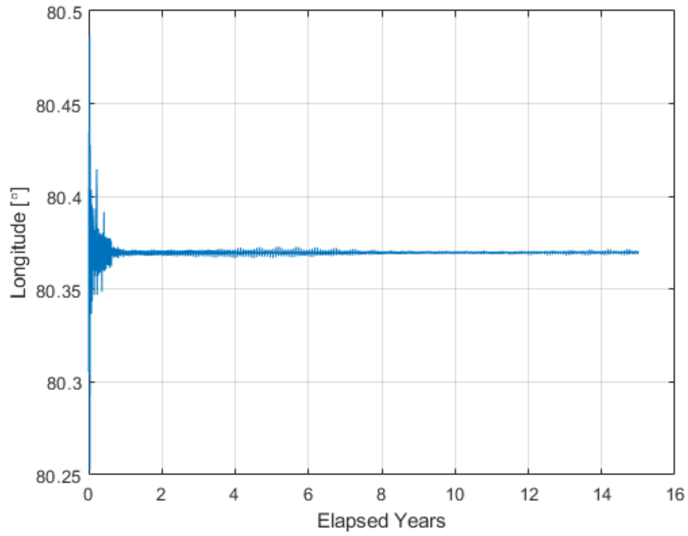

Figure 15: Achieved satellite longitude after station-keeping maneuvers over mission duration for GMAT simulation 2 (GEO with station-keeping).

Validation Results

According to GMAT, the orbit period is p is 86,164 seconds, whilst Kepler's third law predicts: $p = 86,165$, according to equation 2. This is a 0.001% difference, hence, this check was validated.

4.1.2. Shadow Model

With the same geostationary orbit with station keeping as defined above, the shadow model was applied, yielding the following results. The details of the shadow model transition between sunlight, penumbra and umbra are not clearly distinguishable over the mission lifetime of 16, therefore the data was focused around such a regime transition to yield figure 17; this shows the continuous output of the shadow model, shifting from absolute sunlight to penumbra and umbra and back again.

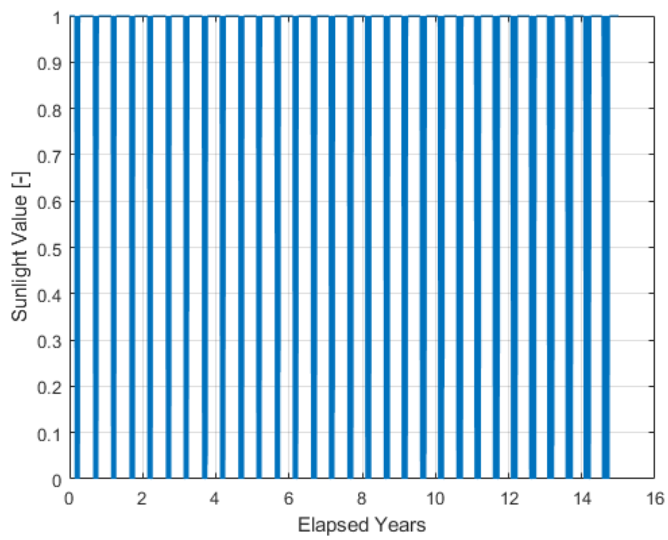

Figure 16: Shadow model results over mission duration for GMAT simulation 2 (GEO with station-keeping).

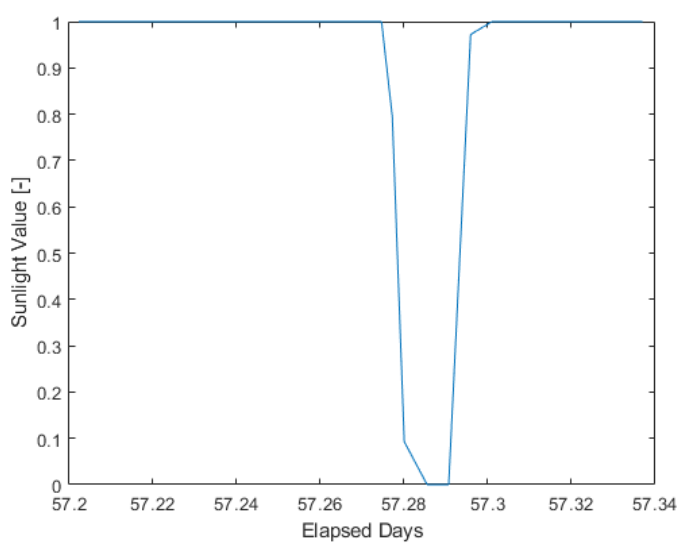

Figure 17: Shadow model results centered over a regime transition for GMAT simulation 2 (GEO with station-keeping).

The figure also indicates limitations due to the timestep resolution of the orbital model, where very few points are available defining the limited period of umbra and penumbra, and highlighting the possibility of skipping such regime transitions if they are short enough; for this reason, it is crucial to pick suitable maximum timesteps of the simulation.

The shadow function plot of figure 16 showed a trend which was repeated over the entire mission duration. By focusing on a yearly basis, such as in figure 18, a trend was found, which is that twice a year, a period where the satellite enters and leaves the Earth's umbra several times a day occurs. This is known as the Eclipse (ECL) season, and occur approximately from late February to mid-April and from late August to mid-October (N.O.A.A, n.d.). The duration of time in the different shadow regimes is detailed in table 5, and indicates that the satellite is almost in constant sunlight over the mission duration.

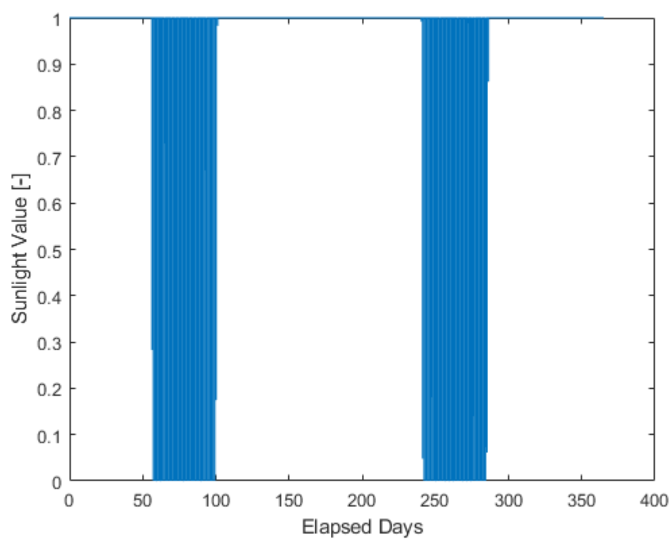

Figure 18: Shadow model results centered over a regime transition for GMAT simulation 2 (GEO with station-keeping).

Table 5: Proportion of time spent in the different shadow and sunlight regimes for GMAT simulation 2 (GEO with station-keeping).

Regime	Proportion of Simulation Duration [%]
Full sunlight	97.0
Penumbra	2.3
Umbra	0.7

Validation Results

Validation of the shadow model was achieved by comparing the results to GMATs "EclipseLocator" function, using the same GEO with station-keeping dataset, but for a 48hr period, beginning on the 27 February 2023 00:00:00 and ending on the 29 Feb 2023 00:00:00, with the results being detailed table 6

The average difference is 3 min 19 seconds; and is likely due to the fact that the "EclipseLocator" does not use the same timesteps as outputted by the GMAT report; the timesteps from the research model are those closest to the GMAT predictions therefore the check was validated.

Table 6: Validation stop times for the different regime transitions for GMAT simulation 2 (GEO with station-keeping).

	Regime Stop Time (UTC)	
Regime	GMAT "EclipseLocator"	Research Model
Sunlight	27 Feb 2023 18:37:18.222	27 Feb 2023 18:38:38.114
Penumbra	27 Feb 2023 18:44:23.730	27 Feb 2023 18:50:34.351
Umbra	27 Feb 2023 18:58:38.720	27 Feb 2023 19:05:33.879
Penumbra	27 Feb 2023 19:05:44.207	27 Feb 2023 19:12:56.858
Sunlight	28 Feb 2023 18:33:55.843	28 Feb 2023 18:35:07.821
Penumbra	28 Feb 2023 18:39:02.221	28 Feb 2023 18:43:34.855
Umbra	28 Feb 2023 19:03:32.192	28 Feb 2023 19:05:34.671
Penumbra	28 Feb 2023 19:08:38.549	28 Feb 2023 19:09:12.831
Sunlight	29 Feb 2023 00:00:00.000	29 Feb 2023 00:00:00.000

4.1.3. Visibility Model

The visibility model was also applied to the same orbit as before. From the ground track of the satellite, a fictional ground station was set in Sri Lanka, with the following geodetic coordinates:

- Latitude: 8.506723°
- Longitude: 80.086386°
- Altitude: 300 m

Figure 19 was obtained as a result and indicates constant line of sight between the satellite and the ground station.

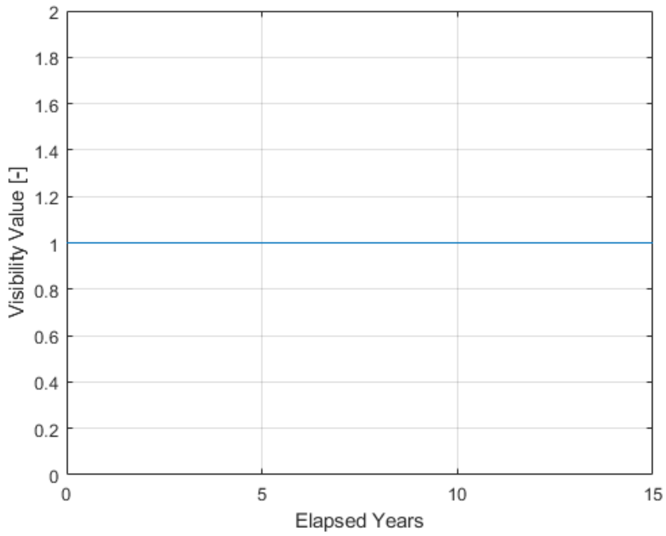

Figure 19: Visibility results over mission for GMAT simulation 2 (GEO with station-keeping).

Validation Results

Geodetic to ECEF conversion: To validate the geodetic to ECEF conversion algorithm used in this paper, 10 positions were converted and the results compared to an online conversion tool developed by the US Naval Postgraduate school's department of Oceanography (N.P.S, n.d.). The average difference was 0.29 %, with a maximum difference of 13 km, details of this are in appendices 7.4; therefore this check was validated.

Visibility model: The visibility model was evaluated by comparing it to GMAT's "ContactLocator" for the year starting 1st Jan 2023, no lack of visibility was recorded in both models, the check is therefore validated.

4.1.4. Degradation Model

Kerslake and Gustasfon (2003) from NASA estimated the rate of degradation for panels on the International Space Station (ISS) to be between 0.2% and 0.5% per year after analysis of solar cell data; with a theoretical model predicting a rate of 0.8% per year. Elsewhere, the ESA (2009) states solar cells on geostationary satellites still retain 88% of their performance after a mission duration of 15 years, which is equivalent to a degradation rate of roughly 0.8% per year. This study chose the worst case scenario for the degradation rate, selecting 0.8% per year to match with NASA's model predictions and ESA data. With this value, the degradation model's values followed the relationship in equation 28, ending with a retention factor of 88.7%; this is shown in 20. Although the relation seems linear, in reality this is an exponential curve, as is shown with a higher rate of degradation of 10% per year in figure 21.

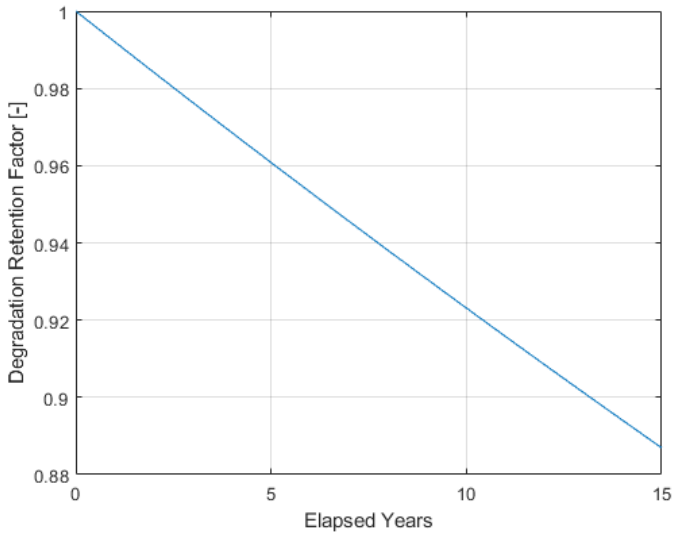

Figure 20: Degradation over mission duration with a degradation rate of 0.8% per year for GMAT simulation 2 (GEO with station-keeping).

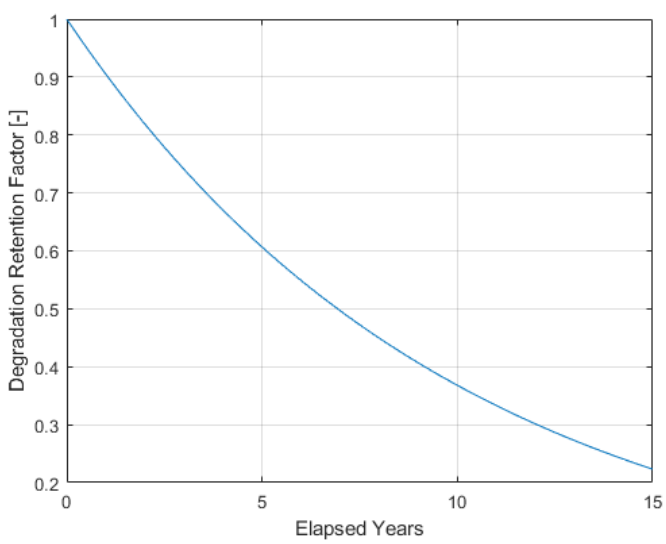

Figure 21: Degradation over mission duration with a degradation rate of 10% per year GMAT simulation 2 (GEO with station-keeping).

4.2. Class I

With the previous models defined and validated, it was possible to examine various SBSP systems using the approach detailed previously. Three concepts were examined: SPS-ALPHA by John Mankins (2012), CASSIOPeiA by Ian Cash (2019), and Multi-Rotary

Joints SPS by Hou et al. (2021); these were chosen as they were considered the leading implementations of SBSP at the time of writing (Frazer-Nash, 2021).

Each of these systems detail a 2 GW variant, this is the value taken for P_{bol}, and were simulated using the same orbit as GMAT simulation 2 (GEO with station-keeping) over a mission lifetime of 15 years.

The produced power over the mission duration is shown in figure 22. It is possible to observe the impacts of degradation from the linear decrease in the maximum power produced, as well as the shadow function with the biannual eclipse periods.

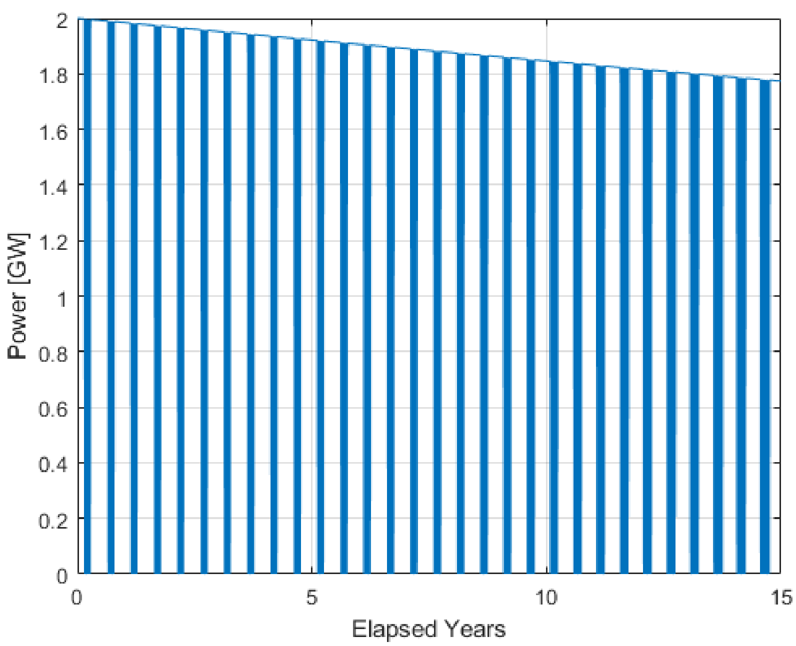

Figure 22: Power production over mission duration for a 2GW SBSP system, using GMAT simulation 2 (GEO with station-keeping).

The yearly average energy produced is 16, 340 million kWh per year; if no degradation were to occur, and the sunlight were constant, the maximum energy produced would be 17, 520 million kWh per year, hence the results produced are on the correct scale. Furthermore, MR-SPS (Hou *et al.*, 2021) reports a yearly output of 7884 million kWh per year based on a 1GW variant, aligning with these predictions. With 0.8% degradation, the minimum power produced in the sunlight was at end of life, at 1.77 GW.

4.3. Class II

Despite having computed the energy generated by existing SBSP concepts, it is valuable to examine how architectural design choices can impact the total energy produced. This section examined the following:

- Orbit Choice: Low Earth Orbit (LEO), Geosynchronous Orbit (GSO), Geostationary Orbit (GEO)

- Degradation Models: high, medium and low degradation rates
- Solar Cells: AzurSpace's 4G32C, Solaero's Z4J and Spectrolab's XTE-SF

4.3.1. Orbit Choice

Assuming the reference system described in the methodology, with an area of 1 km^2 and assuming for the moment a simplified efficiency model with no temperature dependence, with a beginning of life value of 40%, similar to those used in medium-term SBSP implementations: SPS-ALPHA: 48% (Mankins, 2012); CASSIOPeiA: 40% (Cash, 2019); MR-SPS: 40% (Hou *et al.*, 2021), then the power and energy was computed for different orbits. A degradation rate of 0.8% per year was used. LEO, GSO and GEO orbits with parameters detailed in table 7 were simulated for a year.

Table 7: Selected Keplerian orbital elements for GMAT simulation 3 (LEO, GSO, GEO with station-keeping).

Orbital Parameter	LEO	GSO	GEO
SMA	6,734 km	42, 164 km	42,164 km
ECC	0.00005	0	0
INC	35°	10°	0°
RAAN	275°	0°	0°
AOP	0°	0°	0°
TA	221.87°	0.7°	0.7°

The simulations yielded the following results, with the plot of power in figure 23 and ground track in figure 24. It was found that the LEO orbit produced 3.17 million kWh in a year, the GSO orbit produced 2,377 million kWh and GEO produced 2,395 million kWh. This means the GEO orbit produced over 750 times more energy than the LEO orbit and as is due to the shadow and visibility differences, shown in table 8.

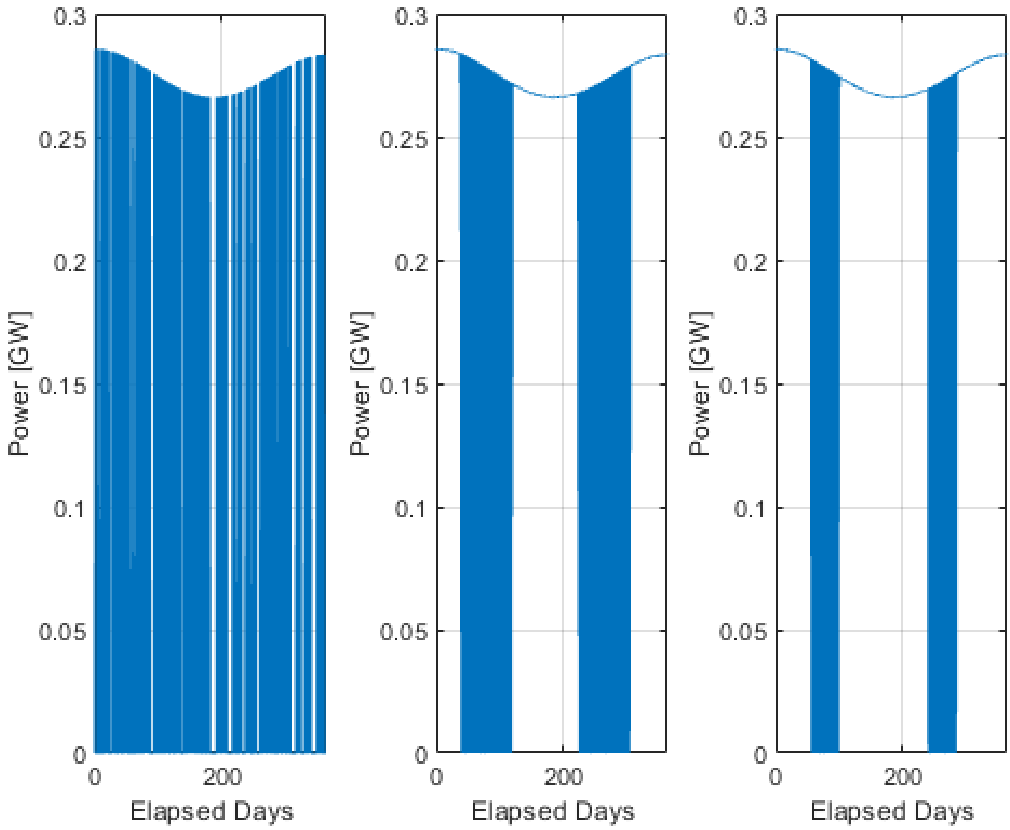

Figure 23: Power production over mission duration for different orbits.

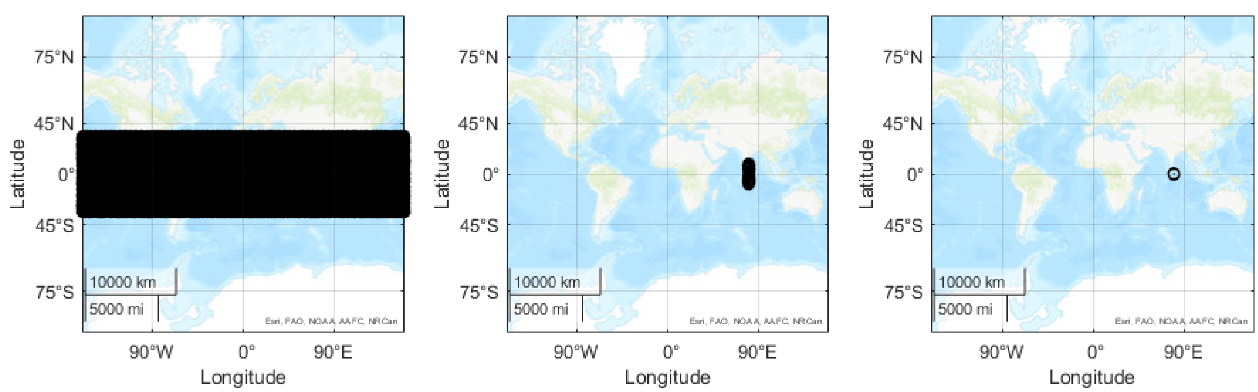

Figure 24: Different ground tracks for LEO, GSO and GEO orbits

Table 8: Proportion of time spent in different regimes for LEO, GSO and GEO over one year.

	Proportion of time [%]		
Regime	LEO	GSO	GEO
Sunlight	62.11	95.55	97.44
Penumbra	0.37	1.07	0.63
Umbra	37.52	3.38	1.93
Visible	0.21	100.0	100.0

4.3.2. Degradation Model Choice

From the previous section, it was determined that the optimal orbit choice for SBSP was GEO; this orbit was then tested with different degradation rates to test their impact on the overall energy generation of the system. Taking a low degradation rate, as reported by NASA for the ISS of 0.2% (Kerslake & Gustasfon, 2003); a medium degradation rate of 0.8% and a high degradation rate to represent the worst case scenario of 3%, as well as a model with no degradation as a baseline; the following results were obtained. The power curves are shown in figure 25, with the resulting energies tabulated in table 9. Although the impact of degradation can be seen in the percentage differences in the energy produced, over one year the difference is minor; this impact becomes exponentially more substantial as the mission duration increases, as can be seen in 26, over 30 years, a slight difference in annual degradation rate creates larger differences, for this reason, accurate selection of degradation rates is critical to accurately predicting the energy output of SBSP systems.

Table 9: Energy production for different degradation rates over one year for GEO with station-keeping.

	NO	LOW	MED	HIGH
Energy [million kWh]	2,405	2,402	2,395	2,369
Difference to baseline	N/A	0.12%	0.41%	1.5%

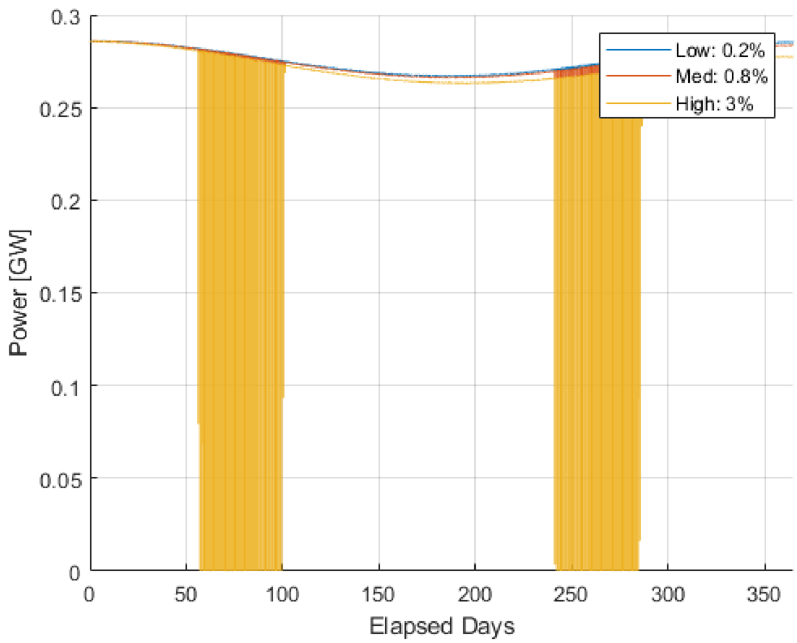

Figure 25: Power production over mission duration for different degradation rates.

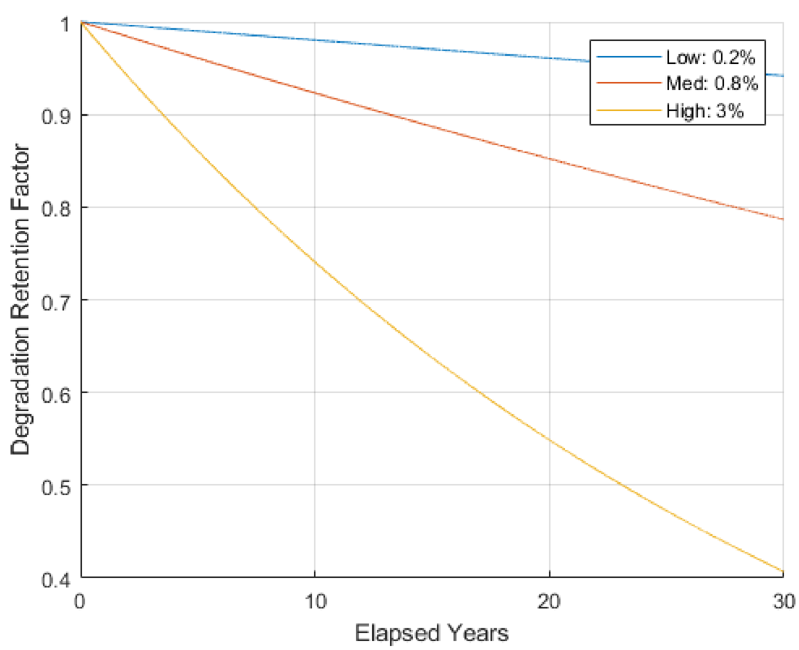

Figure 26: Degradation retention factors for different annual rates over hypothetical 30-yr mission lifetime.

4.3.3. Solar Cell Choice

Using the GMAT 2 GEO orbit with station-keeping dataset, with a mission duration of 15 years; the following solar cells were tested: Azur Space's 4G32C, Solaero's Z4J and Spectrolab's XTE-SF, details of which are available in appendix 7.5. The resulting values of P_{sol} over the mission duration are shown in figure 27 and shows the cyclical variation of the distance between the Sun and the satellite.

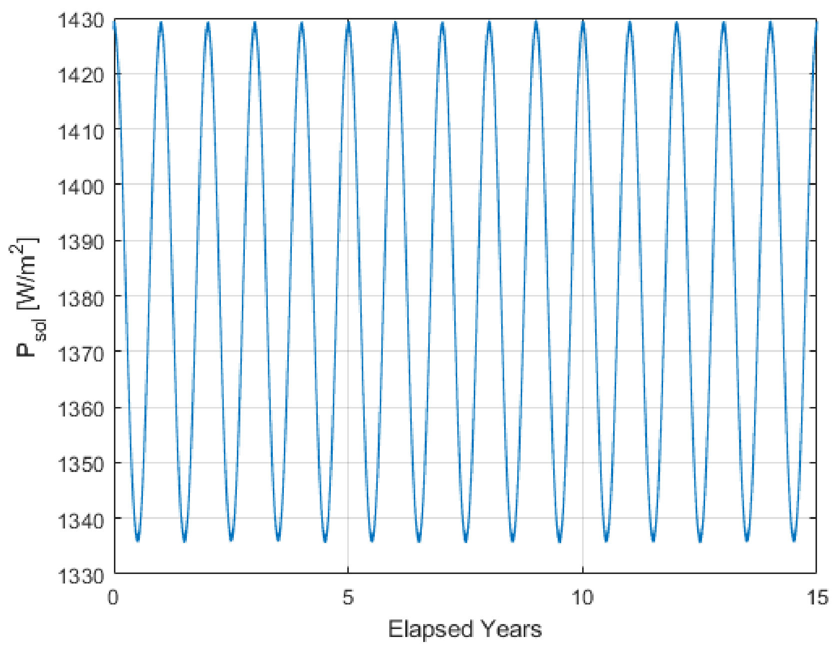

Figure 27: P_{sol} over mission lifetime for GMAT simulation 2 (GEO with station-keeping)

Elsewhere, the results of the temperature model for the Azur Space cell of figure 28 shows a dependence on P_{sol}, and thusly also on the distance between the satellite and the Sun.

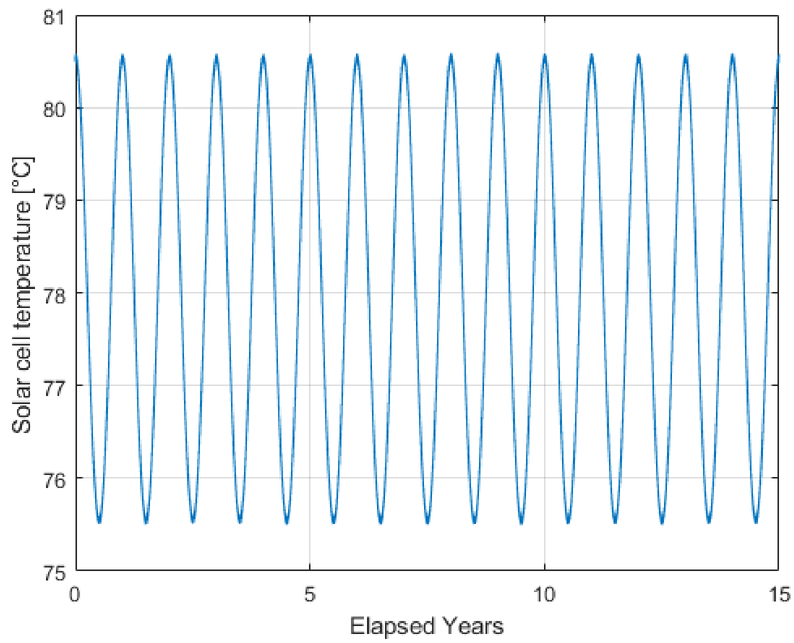

Figure 28: Azur Space solar cell temperature over mission duration

Finally, the power values are plotted in figure 29, this plot was generated by setting $S = 1$ along the entire mission duration so as to have a clearer comparison between the power of each cell (please refer to the previous sections for the shadow model of GMAT simulation 2). The resulting energies with the correctly implemented shadow model are detailed in table 10 and do not indicate large differences, meaning that cell choice does not have a large impact, as most space solar cells have similar characteristics.

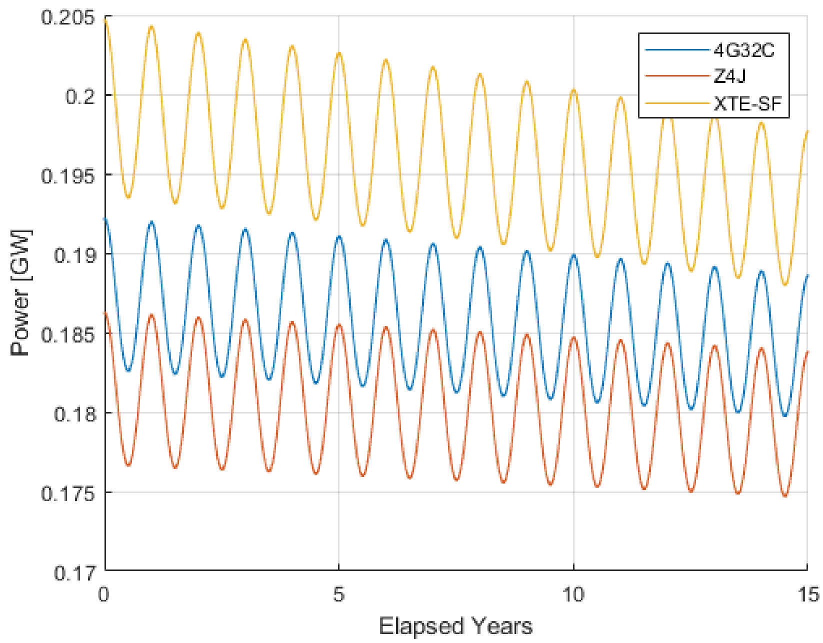

Figure 29: Power generation over mission duration for different cell types, when $S = 1$

Table 10: Energy production for different degradation rates over one year for GEO with station-keeping.

	Azur Space 4G32C	Solaero Z4J	Spectrolab XTE-SF
Total Energy [million kWh]	24,160	23,452	25,499
Average Annual Energy [million kWh]	1,611	1,564	1,700

5. Future Work

5.1. Improvements to the methodology

Whilst this approach to simulating and calculating the energy generation of space-based solar power systems shows potential, there is still work which can be done to improve it. Whilst work could be done to improve each individual model, from the shadow, visibility and degradation models to the power and energy calculations, this would not be a good use of resources as the shadow and visibility are already sufficiently accurate; instead special attention should be given to the degradation model, as well as the obtention of the P_{bol} value when analysing SBSP systems.

Additionally, an expansion of this approach to deal with satellite constellations would be beneficial. In general, SBSP systems become more cost-effective with economies at scale, although only 3 satellites would be needed for global coverage, it is not unreasonable to assume constellations of 5 satellites providing power to multiple ground stations, which could be modelled with some modifications to the visibility model and the GMAT orbital model. Adding such functionality could also make simulations of cluster concepts of SBSP possible, such as Ryan McLinko and Basant Sagar's distributed network of satellites for efficient space power transmission (2010).

Finally, further work could be done to integrate the computations with the results from GMAT's orbital model. GMAT's Python API is currently under development, and could lead to a more streamlined approach, allowing the interaction with GMAT to be purely programmatic, and could be directly called from Python.

5.2. sspPy - A python package

During the course of this research, a python library named Space Solar Power (sspPy) integrating the methods described in this paper has been developed and is available for download from the Python Package Index (PyPi). It allows users to replicate the results of this study, and simulate any SBSP concept provided the relevant data is inputted. Further work can be done to speed up the computations, vectorizing the operations where possible, as well as general development of the documentation and additional functionality such as constellation modelling.

6. Conclusion

This research aimed to establish methods for calculating the energy generation potential of space-based solar power systems, this was achieved through a simulation and model-based approach which computed the power of the system at every timestep and converted this to energy.

The difficulties of modelling such systems arise in part from their hypothetical nature, with SBSP being researched since 1968, but with no real-world demonstration let alone full-scale implementation existing at the time of writing. This means real-world data is inexistant, and a purely theoretical approach must be undertaken, with no possibility of validating the generated results with empirical data, or even deriving models from such data.

During the study, two main classes of solution for power computations were developed, with the first allowing computations relating to fully-conceptualised space-based solar power implementations based solely on a single technical parameter P_{bol}. This allowed for a straightforward way to calculate the energy of such systems, and the method was also generalizable, being able to represent complex systems with many components in a single value. This did come with inherent limitations, relying on this value to be accurate, but also reliant on assumptions which could not always be verified, such as assuming P_{bol} to be the beginning of life power capacity instead of the mission lifetime. However, the model showed promising findings that aligned with back-of-the-hand predictions used by cost-benefit studies.

The second method was developed with the main goal of conducting sensitivity analyses of space-based solar power systems by creating an approach which had to be fundamentally more complex in order to be able to select and model the impacts of different parameters in the system. This meant additional models needed to be developed, notably a model of a solar cell which in turn necessitated a thermal model, whilst other components like the orbit and degradation choices could be studied using work done for the first class of solution but expanded to different scenarios and values. This also came with limitations, as the individual models of solar cells and temperature were simplified and could differ from reality. However, as a result of this model, information relating to the impacts of specific components of the system could be determined, which can guide future improvements to this approach by indicating the factors with the greatest potential to vary the results significantly, such as the orbit choice and degradation rates.

Although these limitations exist, special care was taken to limit the assumptions made whilst developing the models, and at each possible stage, validation tests were conducted to examine the results of individual models. Equally, comparisons were made with idealised and simplified scenarios to make sure the scale of the results matched expectations, this was done notably when examining the resulting power and energy values over different mission durations with the theoretical maximum.

From this research, it was found that although the back-of-the-hand predictions simplifying SBSP systems can produce results with a similar order of magnitude as in this approach, there can also be significant deviations on the order of 3.5% (compared to MR-SPS's predictions (Hou *et al.*, 2021)) and 7% (compared to Frazer-Nash's cost-benefit study (2021)), which have the potential to alter the findings of such studies; highlighting the need for accurate modelling.

Finally, this is the first study into calculating the energy potential of SBPS systems, and future work can be done to improve the results. Although this approach as a whole shows promise and results which are in-line with expectations, future work can improve components of this research, focusing for example on the thermal model, which contains a steady-state assumption not used in more complex and accurate thermal models of spacecraft found in the literature. Future work can also be done to increase the user-friendliness and speed of computation of the release Python package sspPy as discusses in section 5.2.

In conclusion, this study established approaches allowing the computation of power and energy generation potential of space-based solar power (SBSP) systems. Whilst acknowledging the inherent challenges with simulating such systems, this research developed two models which can calculate the power and energy of these systems, but future work can be done to improve these. By building upon this foundation, it will be possible to accurately predict the potential of these systems and conduct more accurate cost-benefit analyses, which might one result in the development of a real-world implementation.

Acknowledgments

I would like to express my deepest gratitude to my supervisor, Dr. Panagiotis Angeloudis, for his invaluable guidance and unwavering support. I would also like to express my heartfelt appreciation to my family for their constant love and support. And finally, thank you to Edgar Zapata and Ian Cash for their patience in answering my questions.

References

Anderson, P. (2015) Operational Considerations of GEO Debris Synchronization Dynamics. *International Aeronautical Federation*. https://hanspeterschaub.info/Papers/Anderson2015c.pdf [Accessed 10/06/2023].

Ansys (n.d.) *Maintaining GEO Slot*. https://help.agi.com/stk/#training/Astro_MaintGeoSlot.htm [Accessed: 9/06/2023].

Asimov, I. (1941) *Reason*. New York, Street and Smith Publications Inc.

AzurSpace (2019) *32% Quadruple Junction GaAs Solar Cell*. https://www.azurspace.com/images/0005979-01-01_DB_4G32C_Advanced.pdf [Accessed: 10/06/2023].

Bentley (n.d.) *Useful Concepts*. https://docs.bentley.com/LiveContent/web/ContextCapture%20Cloud%20Processing%20Console%20Help-v3/en/GUID-E526248D-E27D-41C4-9CA2-97E9FBBE5CC5.html [Accessed: 10/06/2023].

Borthomieu, Y. (2014) *Satellite Lithium-Ion Batteries*. In: Pistoia, G. (ed.) *Lithium-Ion Batteries*, Elsevier, pp. 311-344. https://doi.org/10.1016/B978-0-444-59513-3.00014-5.

Bozek, J. M. & Oleson, S. R. (1993) *Comparisons of Selected Laser Beam Power Missions to Conventionally Powered Missions*. N.A.S.A. https://space.nss.org/wp-content/uploads/1993-Comparisons-Of-Selected-Laser-Beam-Power-Missions.pdf [Accessed: 10/06/2023].

Cash, I. (2019) *CASSIOPeiA - A new paradigm for space solar power*. https://www.spaceenergyinitiative.org.uk/wp-content/uploads/2021/09/CASSIOPeiA-A-New-Paradigm-for-SSP.pdf [Accessed: 10/06/2023].

Clynch, J. R. (2002) *Geodetic Coordinate Conversions*. https://www.oc.nps.edu/oc2902w/coord/coordcvt.pdf [Accessed: 10/06/2023].

Darling, D. (n.d.) *Station-Keeping*. https://www.daviddarling.info/encyclopedia/S/station-keeping.html [Accessed: 10/06/2023].

E.S.A (2009) *Inside a solar cell*. https://www.esa.int/Enabling_Support/Space_Engineering_Technology/Inside_a_solar_cell [Accessed: 10/06/2023].

E.S.A (n.d.) *Cost vs. benefits studies*. https://www.esa.int/Enabling_Support/Space_Engineering_Technology/SOLARIS/Cost_vs._benefits_studies [Accessed: 10/06/2023].

Etchells, T. & Berthoud, L. (2019) Developing a Power Modelling Tool for CubeSats. *American Institute of Aeronautics and Astronautics*. https://digitalcommons.usu.edu/

cgi/viewcontent.cgi?article=4336&context=smallsat [Accessed: 10/06/2023].

Evans, D. L. & Florschuetz, L. W. (1977) Cost studies on terrestrial photovoltaic power systems with sunlight concentration. *Solar Energy*. 19 (3), 255-262. https://www.sciencedirect.com/science/article/abs/pii/0038092X77900688?fr=RR-2&ref=pdf_download&rr=7d68b6113e6d71de [Accessed: 10/06/2023].

Field, M. (21st February 2021) *The budget space race is poised for take-off*. The Telegraph. https://www.telegraph.co.uk/technology/2021/02/20/budget-space-race-poised-take-off/ [Accessed: 10/06/2023].

Frazer-Nash (2021) *Space Based Solar Power*. https://www.fnc.co.uk/media/e15ing0q/frazer-nash-sbsp-executive-summary-final.pdf [Accessed: 10/06/2023].

Fritts, C. E. (1883) On a New Form of Selenium Cell, and Some Electrical Discoveries Made by Its Use. *American Journal of Science*. s3-26 (156), 465-472. https://ajs.scholasticahq.com/article/65415 [Accessed: 10/06/2023].

Glaser, P. (1968) Power from the Sun: Its Future. *Science*. 162 (3856), 857-861. https://doi.org/10.1126/science.162.3856.857 [Accessed: 10/06/2023].

Goodyer, J. (21th April 2022) *NASA to test giant slingshot designed to fling satellites into orbit*. BBC Science Focus. https://www.sciencefocus.com/news/nasa-to-test-giant-slingshot-designed-to-fling-satellites-into-orbit/ [Accessed: 10/06/2023].

Gorev, V. N., Prokopiev, V. Y., Prokopiev, Y. M., Sinitsina, L. D. & Sidorchuck, A. A. (2019) Calculating electric power generated by 3U CubeSat's photoconverters depending the orbit and orientation parameters. *IOP Conference Series: Materials Science and Engineering*. 537 (1). https://doi.org/10.1088/1757-899X/537/2/022079 [Accessed: 10/06/2023].

Gosavi, S. S., Mane, H. G., Pendhari, A. S., Magdum, A. P., Deshpande, S., Baraskar, A., Jadhav, M., & Husainy, A. (2021) A Review on Space Based Solar Power. *Journal of Thermal Energy System*. 6 (1). https://doi.org/10.46610/JoTES.2021.v06i01.003 [Accessed: 10/06/2023].

Honsberg, C. & Bowden, S. (n.d.) *PV Education*. https://www.pveducation.org/ [Accessed: 10/06/2023].

Hou, X., Li, M., Niu, L., Zhou, L., Chen, Y., Cheng, Z. & Ji, H. (2021) SunSat Design Competition 2014-2015 First Place Winner - Team CAST: Multi-Rotary Joints SPS. *Online Journal of Space Communication*. 11 (8). https://ohioopen.library.ohio.edu/spacejournal/vol11/iss18/4/?utm_source=ohioopen.library.ohio.edu%2Fspacejournal%2Fvol11%2Fiss18%2F4&utm_medium=PDF&utm_campaign=PDFCoverPages [Accessed: 10/06/2023].

Jain, A. & Trost, N. (n.d.) Current and Near-Future Space Launch Vehicles for Manned Trans-Planetary Space Exploration: Phobos-Deimos mission architecture case study. *American Institute of Aeronautics and Astronautics.* `https://sicsa.egr.uh.edu/sites/sicsa/files/files/publications/aiaa2013.pdf` [Accessed: 10/06/2023].

Johnson, W. N., Akins, K., Armstrong, J., Cheung, K., Henshaw, G., Huynh, S., Jaffe, P., Long, M., Mook, M., Osborn, M., Skalitzky, R., Tasker, F., Dahlburg, J., Lovelette, M. N., Bartolo, R., Williams, K., Dorsey, M., Gubser, D., Jenkins, P., Messenger, S., Pasour, J., Walters, R., Smith, N., Boncyk, W., Brown, M. & Huber, D. (2009) *Space-based Solar Power: Possible Defense Applications and Opportunities for NRL Contributions.* Naval Research Laboratory. Report number: NRL/FR/7650–09-10,179. `https://www.researchgate.net/publication/235216367_Space-based_Solar_Power_Possible_Defense_Applications_and_Opportunities_for_NRL_Contributions` [Accessed: 10/06/2023].

Jones, H. (2018) The Recent Large Reduction in Space Launch Cost. *International Conference on Environmental Systems.* 2018 (81). `https://ttu-ir.tdl.org/bitstream/handle/2346/74082/ICES_2018_81.pdf` [Accessed: 10/06/2023].

Kerslake, T. & Gustafson, E. (2003) *On-Orbit Performance Degradation of the International Space Station P6 Photovoltaic Arrays.* N.A.S.A. `https://ntrs.nasa.gov/api/citations/20030068268/downloads/20030068268.pdf` [Accessed: 10/06/2023].

Kim, H. & Han, C. (2010) Analytical and numerical approaches of a solar array thermal analysis in a low-earth orbit satellite. *Advances in Space Research.* 46 (2010), 1427-1439. `DOI:10.1016/j.asr.2010.08.023` [Accessed: 10/06/2023].

Landis, G. (1994) *Review of Solar Cell Temperature Coefficients for Space.* N.A.S.A. `https://ntrs.nasa.gov/api/citations/19950014125/downloads/19950014125.pdf` [Accessed: 10/06/2023].

Lewis-Weber, J. (2016) Lunar-Based Self-Replicating Solar Factory. *New Space.* 4 (1), 53-62. `https://doi.org/10.1089/space.2015.00413` [Accessed: 10/06/2023].

Mankins, J. (1997) *A Fresh Look at Space Solar Power: New Architectures, Concepts and Technologies.* N.A.S.A. `https://space.nss.org/wp-content/uploads/1997-Mankins-Fresh1Look1At1Space1Solar1Power.pdf` [Accessed: 10/06/2023].

Mankins, J. (2012) *SPS-ALPHA: The First Practical Solar Power Satellite via Arbitrarily Large Phased Array.* N.A.S.A. `https://www.nasa.gov/pdf/716070main_Mankins_2011_PhI_SPS_Alpha.pdf` [Accessed: 10/06/2023].

McLinko, R. & Basant, S. (2010) Space-based solar power generation using a distributed network of satellites and methods for efficient space power transmission. In: Ma, X., Yang, B. & Li, M. (eds.) *International Conference on Space Information Technology*, The

International Society for Optical Engineering. http://dx.doi.org/10.1117/12.855381.

Messenger, S. R., Summers, G. P., Burker, E. A., Walters, R. J. & Xapsos, M. A. (2000) Modeling Solar Cell Degradation in Space: A Comparison of the NRL Displacement Damage Dose and the JPL Equivalent Fluence Approaches. *Progress in Photovoltaics: Research and Applications*. 2001 (9), 103-121. https://doi.org/10.1002/pip.357 [Accessed: 10/06/2023].

Mollick, A. (n.d.) *Why it's crucial to understand the fill factor of solar cell? How it's affecting the efficiency of PV cells?*. https://ecowowlife.com/fill-factor-of-solar-cell/ [Accessed: 10/06/2023].

Montenbruck, O. & Gill, E. (2001) *Satellite Orbits: Models, Methods and Applications (2nd ed.)*. Berlin, Springer DE.

Nadir, B. (2003) *16.851: Satellite Engineering*. https://ocw.mit.edu/courses/16-851-satellite-engineering-fall-2003/533672f84f6c6e3054730b672d53c87b_portfolio_nadir1.pdf [Accessed: 10/06/2023].

N.A.S.A (1978) *Satellite Power System: Concept Development and Evaluation Program*. https://space.nss.org/wp-content/uploads/SSP-DOE-1978-space-solar-power-Reference-System-Report.pdf [Accessed: 10/06/2023].

N.A.S.A (2014) *Measuring Earth's Albedo*. https://earthobservatory.nasa.gov/images/84499/measuring-earths-albedo#:~:text=Changes%20in%20ice%20cover%2C%20cloudiness,albedo%20is%20about%20about%200.30 [Accessed: 10/06/2023].

N.A.S.A (n.d.) *General Mission Analysis Tool (GMAT) v.R2016a*. https://software.nasa.gov/software/GSC-17177-1 [Accessed: 10/06/2023].

N.O.A.A (n.d.) *GOES Eclipse Schedule*. https://www.ospo.noaa.gov/Operations/GOES/eclipse.html#:~:text=GOES%20satellites%20encounter%20two%20periods,maximum%20of%2072%20minutes%20daily [Accessed: 10/06/2023].

N.P.S (n.d.) *Latitude,Longitude,Height to/from ECEF (X,Y,Z)*. https://www.oc.nps.edu/oc2902w/coord/llhxyz.htm [Accessed: 10/06/2023].

N.R.E.L (n.d.) *Solar Energy Basics (Text Version)*. https://www.nrel.gov/news/video/solar-energy-basics-text.html#:~:text=Humans%20first%20directly%20harnessed%20solar,by%20American%20inventor%20Charles%20Fritts [Accessed: 10/06/2023].

Olds, J. (1998) *Launch Vehicle Assessment for Space Solar Power*. N.A.S.A. https://ntrs.nasa.gov/api/citations/19990018029/downloads/19990018029.pdf [Accessed: 10/06/2023].

Oleson, S. (1999) *Advanced Electric Propulsion For Space Solar Power Satellites. Re-*

port number: 209307. N.A.S.A. https://space.nss.org/wp-content/uploads/1999-Advanced1Electric1Propulsion1For1SPS.pdf [Accessed: 10/06/2023].

Phen, A. (2022) *The realization of a study on the current status and future trends of the cost of access to space for CubeSat missions*. Luleå University of Technology. http://ltu.diva-portal.org/smash/get/diva2:1715413/FULLTEXT01.pdf [Accessed: 10/06/2023].

Proctor, N., Eggert, R., Lange, I., Madrid, A., & Maniloff, P. (n.d.) *21st Century Trends in Space-Based Solar Power Generation and Storage*. N.A.S.A. https://www.nasa.gov/sites/default/files/atoms/files/21st_century_trends_in_space-based_solar_power_generation_and_storage.pdf [Accessed: 10/06/2023].

Rochester (n.d.) *Coordinate Systems*. http://dirsig.cis.rit.edu/docs/new/coordinates.html#:~:text=The%20Earth%2DCentered%2C%20Earth%2DFixed%20(ECEF)%20Coordinate%20System,-The%20Earth%2DCentered&text=It%20is%20a%20simple%20Cartesian,to%20%2BX%20and%20%2BZ [Accessed: 10/06/2023].

Smitherman, D. (n.d.) *A Comparison of a Solar Power Satellite Concept to a Concentrating Solar Power System*. N.A.S.A. https://ntrs.nasa.gov/api/citations/20140003205/downloads/20140003205.pdf [Accessed: 10/06/2023].

Solaero (n.d.) *Z4J Space Solar Cell*. https://www.rocketlabusa.com/assets/Uploads/RL-SolAero-Data-Sheet-Z4J.pdf [Accessed: 10/06/2023].

SpaceAcademy (n.d.) *Satellite Orbital Lifetimes*. https://www.spaceacademy.net.au/watch/debris/orblife.htm [Accessed: 10/06/2023].

Spectrolab (n.d.) *32.2% XTE-SF (Standard Fluence)*. https://www.spectrolab.com/photovoltaics/XTE-SF%20Data%20Sheet%20_07.27.22.pdf [Accessed: 10/06/2023].

S.R.A. (1985) *Solar Power Satellite Built of Lunar Materials*. Space Studies Institute. https://space.nss.org/wp-content/uploads/1985-SPS-Lunar-Materials-Study.pdf [Accessed: 10/06/2023].

Tandle, S. (2019) *Space-Based Solar Power Station*. Deggendorf Institute of Technology. http://dx.doi.org/10.13140/RG.2.2.14525.49123 [Accessed: 10/06/2023].

Vanderbilt (n.d.) *Kepler's Third Law*. https://www.vanderbilt.edu/AnS/physics/astrocourses/ast201/keplerslaws_3.html [Accessed: 10/06/2023].

Vedda, J. A. & Jones, K. L (2020) *Space-Based Solar Power: A Near-Term Investment Decision*. Center for Space Policy and Strategy. https://aerospace.org/sites/default/files/2020-10/Vedda-Jones_SolarPower_20201006_0.pdf [Accessed: 10/06/2023].

Wilcox, J. R. (2013) *Solar Cell Temperature Dependent Efficiency and Very High Tempera-*

ture Efficiency Limits. Open Access Dissertations. https://docs.lib.purdue.edu/cgi/viewcontent.cgi?article=1198&context=open_access_dissertations [Accessed: 10/06/2023].

Winston, R., Minano, J. C. & Benitez, P. (2005) *Applications to Solar Energy Concentration*. In: Winston, R., Minano, J. C. & Benitez, P. (eds.) *Nonimaging Optics*, Elsevier, pp. 317-394. https://doi.org/10.1016/B978-012759751-5/50013-0.

Zapata, E. & Olds, J. (1999)) Spaceport Operations Assessment for Space Solar Power Earth to Orbit Transportation Requirements. *International Astronautical Federation*. 99. https://space.nss.org/wp-content/uploads/1999-Spaceport-Operations-Assessment-For-Space-Solar-Power.pdf [Accessed: 10/06/2023].

7. Appendices

7.1. Coordinate Systems

GMAT possesses several coordinate systems, the two used in this study are EarthMJ2000Eq and Earth-Fixed.

EarthMJ2000Eq

EarthMJ2000Eq is an inertial coordinate system where the x-axis points along the line formed by the intersection of the Earth's mean equatorial plane and the mean ecliptic plane, in the direction of Aries; the z-axis is normal to the Earth's mean equator and the y-axis completes the right-handed system (N.A.S.A, n.d.). This coordinate system is also referenced at a specific point in time, specifically at the J2000 epoch, which is near noon on the 1st January 2000. In practice, because the center of this coordinate system is aligned with the center of the Earth, the positions of the Earth will always be (0, 0, 0) in three dimensions.

Earth-Centered, Earth-Fixed (ECEF)

ECEF is a simple cartesian coordinate system where the x-axis passes through the Equator and Prime Meridian intersection, the z-axis passes through the North Pole and the y-axis is orthogonal to the x and z axes (Rochester, n.d.), as illustrated in figure 30. This coordinate system rotates with the Earth, and so is particularly useful for tracking geostationary objects like satellites (Rochester, n.d.).

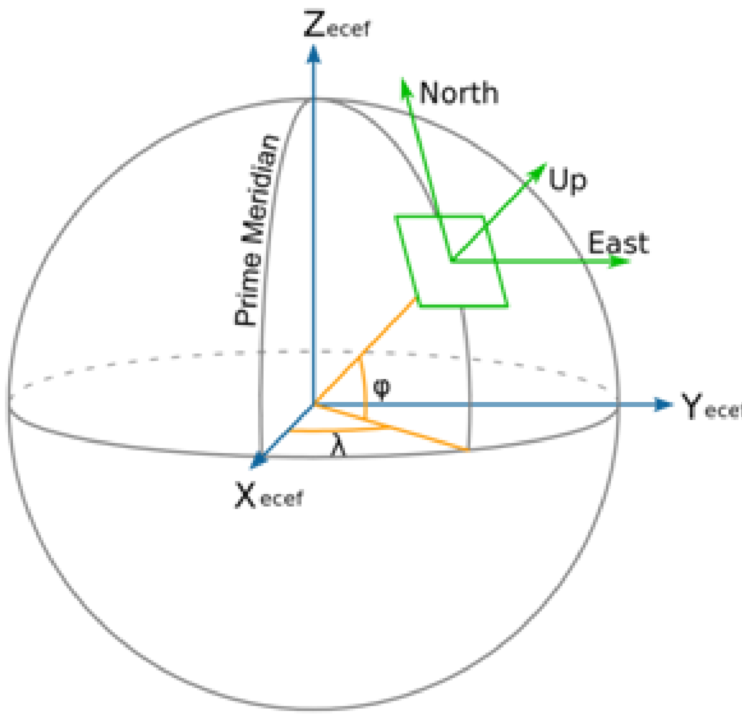

Figure 30: Earth's globe with an ECEF coordinate system (courtesy: Bentley (n.d.).

7.2. Station Keeping Algorithms

The Low Earth Orbit station-keeping algorithm provided in GMAT is detailed in algorithm 2:

Algorithm 2 Low Earth Orbit: Station Keeping

```
while ElapsedDays < SimulationDuration do
    Propagate one step
    if Altitude < Threshold then
        Propagate to periapsis
        while AcheivedRMAG <|> Tol do
            while AcheivedECC <|> Tol do
                Vary ThrusterBurn1
                Apply ThrusterBurn1
                Propagate to apoapsis
                Acheive RMAG
                Vary ThrusterBurn2
                Apply ThrusterBurn2
                Acheive ECC
            end while
        end while
    end if
end while
```

7.3. Electrical circuit parameters

The following are definitions of the parameters used in this study to describe the electrical circuit equivalent of a solar cell, graphically these definitions are illustrated by figure 31.

Short-Circuit Current: I_{sc}

The short-circuit current is due to the generation and collection of light-generated carriers, and is the largest current which may be drawn from the solar cell (Honsberg & Bowden, n.d.). This occurs when there is no voltage. Often, manufacturers list the short-circuit current density J_{sc} which has units of mA/cm^2.

Open-Circuit Current: V_{oc}

The open-circuit voltage, V_{oc}, is the maximum voltage available from a solar cell, and this occurs at zero current (Honsberg & Bowden, n.d.). Typically this decreases with temperature.

Fill Factor: FF

The fill factor is a parameter which, in conjunction with V_{oc} and I_{sc}, determines the maximum power from a solar cell (Honsberg & Bowden, n.d.); as the short-circuit and open-circuit currents are obtained when no power is generated from the cell (as either the current or the voltage is null when these are obtained).

Voltage at Maximum Power: V_{mp}

This is the voltage obtained when the solar cell is operating at its maximum capacity.

Current at Maximum Power: I_{mp}

This is the current which runs through the solar cell when the maximum power is being produced. Just like the short-circuit current, this is often given by manufacturers as the density which has units of mA/cm^2.

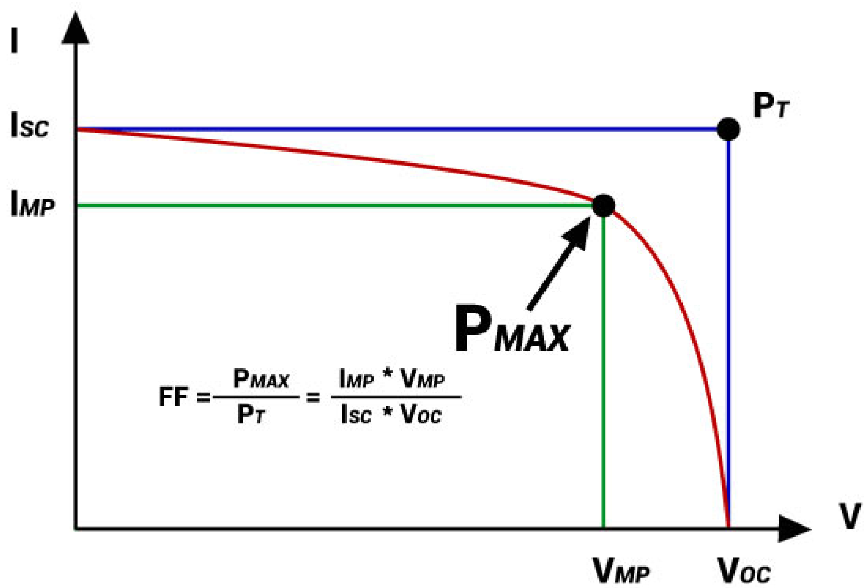

Figure 31: Graph of electrical circuit parameters (courtesy: Mollick (n.d.).

7.4. Geodetic to ECEF: Validation results

Table 11: Geodetic to ECEF validation results.

Geodetic	Earth-Centred Earth-Fixed	
	N.P.S.	Research Model
28.3, -85.3, 213.1	457.8, -5600.6, 3007.4	457.6, -5598.5, 3016.4
-28.5, -53.2, 660.9	3354.9, -4494.0, -3029.0	3353.6, -4492.2, -3038.1
86.4, 100.5, 393.7	-72.5, 390.5, 6344.8	-72.4, 389.9, 6355.5
-85.1, 74.6, 427.5	142.3, 518.5, -6334.5	142.1, 517.7, -6345.2
52.0, -81.8, 257.4	558.3, -3887.4, 5009.0	557.7, -3883.3, 5020.7
1.4, -164.2, 451.3	-6135.9 -1734.9, 161.3	-6135.9, -1734.9, 161.8
-17.4, 70.7, 270.3	2010.9, 5743.5, -1904.5	2010.6, 5742.7, -1910.6
-74.3, 107.4, 914.1	-515.0, 1642.7, -6121.7	-514.2, 1640.1, -6132.8
60.0, -43.6, 272.7	2312.0, -2202.6, 5502.9	2309.1, -2199.8, 5514.5
71.5, 166.8, 354.8	-1974.2, 459.6, 6027.5	-1971.3, 458.9, 6038.6

7.5. Selected solar cells

The parameters were either directly taken from the datasheets (electrical data and temperature gradients) or derived using datasheet parameters (degradation retention factors).

Azur Space: 4G32C

The datasheet is available here (AzurSpace, 2019). This cell type is an AlInGaP/AlInGaAs/InGaAs/Ge on Ge substrate quadruple junction solar cell with a size of 30.18 cm^2 (AzurSpace, 2019).

Solaearo: Z4J

The datasheet is available here (Solaero, n.d.). This cell type is a 4-junction n-on-p on a germanium substrate (Solaero, n.d.).

Spectrolab: XTE-SF

The datasheet is available here (Spectrolab, n.d.). This is a triple junction solar cell with sizes of 27 cm^2 and 77 cm^2 available. (Spectrolab, n.d.).